THESIS FOR THE DEGREE OF LICENTIATE OF ENGINEERING

Determining the Fate and Operational Implications of Alkalis in Chemical Looping Combustion of Biomass

IVAN GOGOLEV

Department of Space, Earth and Environment

CHALMERS UNIVERSITY OF TECHNOLOGY

Gothenburg, Sweden 2020

Determining the Fate and Operational Implications of Alkalis in Chemical Looping Combustion of Biomass

IVAN GOGOLEV

Department of Space, Earth and Environment
Division of Energy Technology
Chalmers University of Technology
SE-412 96 Gothenburg
Sweden
Telephone + 46 (0)31-772 5252

Printed by Chalmers Reproservice
Gothenburg, Sweden 2020

Determining the Fate and Operational Implications of Alkalis in Chemical Looping Combustion of Biomass

IVAN GOGOLEV
Division of Energy Technology
Department of Space, Earth and Environment
Chalmers University of Technology

Abstract

Chemical looping combustion (CLC) of biomass is a promising thermal conversion technology with integrated carbon capture. As with other fluidized bed fuel conversion processes, biomass CLC may be susceptible to issues of agglomeration, fouling and corrosion stemming from the release of alkalis during fuel conversion. How alkalis are released and what implications they have on CLC operation is currently largely unknown. The experimental studies presented in Papers I - III of this thesis aimed at addressing this knowledge gap.

Measurement of gas-phase alkali release in CLC was addressed through the design and construction of a modular and transportable surface ionization detector (SID) system, customized for alkali emissions measurement from the fuel reactor (FR) and the air reactor (AR) of CLC pilots. Gas-phase alkali emissions measurement showed that approximately 1-10% of fuel alkalis are released to the gas phase in CLC. The FR alkali emissions were found to rise with the fuel's alkali content, while no definitive correlation was established for AR emissions. With respect to emissions distribution, AR emissions were found to be generally lower than that of the FR. Surprisingly, in several cases, AR emissions were equal or marginally higher than in the FR. Analysis presented in Paper III led to a preliminary conclusion that AR gas-phase alkali emissions likely occur due to char or ash carryover from the FR, whereby the transported alkali compounds release to the gas phase at the higher temperatures of the AR.

Papers I-III also established that >97% of fuel alkalis are retained in solid form. Although a major part of the alkali retention originates from fuel ash formation, significant retention likely occurs due to oxygen carrier interaction with the fuel's inorganic content. In Paper III it was also found that in CLC, the steam-rich FR atmosphere enhances the gas-phase release of alkalis from decomposition of alkali carbonates and sulphates. This was established in tests comparing CLC operation with oxygen carrier aided combustion (OCAC).

Development of biomass CLC technology was also addressed in this thesis. Paper I demonstrated that gas conversion efficiencies of >96% can be achieved with mixed synthetic and natural oxygen carriers. Experiments in Paper II commissioned a new 10 kW CLC pilot and demonstrated that the implementation of a volatiles distributor in the FR can improve fuel gas conversion efficiency by up to 10 percentage points. Papers I and II also evaluated the interdependencies of the CLC system's control parameters with gas-phase alkali release. It was concluded that CLC system control parameters, other than temperature, likely do not significantly influence and are not constrained by alkali release behavior.

Keywords: chemical looping combustion, alkali release, biomass, carbon capture

ACKNOWLEDGEMENTS

I would like to thank Professors Anders Lyngfelt and Tobias Mattisson for creating the opportunity for my participation in the ash chemistry project, and for creating a truly impressive experimental research infrastructure at Chalmers. I would also like to thank Professor Lyngfelt for his feedback on my work and papers, for his patience, and for his help in improving my understanding of the inner workings of Chalmers and the Energiteknik division.

I would like to thank Associate Professor Carl Linderholm for his efforts in helping me find my way at the division and for his feedback on my scientific work. I would also like to thank Dr. Linderholm for his effort to understand my viewpoints and the personality that drives me and my work.

I would like to acknowledge the funding agencies who made this research possible. The work presented in this thesis was supported by funding from the Swedish Research Council, project "Biomass combustion chemistry with oxygen carriers", contract 2016-06023, and by the Swedish Energy Agency (grant number P43936-1) via the OxyCar-FBC project, which is a project performed within the framework of ERA-NET Bioenergy. Rebuild of 10 kW unit was supported by Carl Tryggers Stiftelse, contract CTS 14:285.

Furthermore, I would like to thank Ulf Stenman for his dedication to helping me and other PhD students achieve success in our experimental work. Ulf is a true professional and a wonderful colleague. I would also like to thank my colleagues Amir, Jesper, Matthias, Patrick, Daofeng, the three Viktors, Fredrick, Ivana, and other members of the CLC and Energiteknik family for your collaboration and companionship.

Last but most, I would like to sincerely thank my sambo Maria for being brave and taking on the challenge of moving to Sweden, and for all of her support throughout my time at Chalmers.

List of Publications Included in the Thesis

This thesis is based on the following three appended papers:

I. Gogolev, Ivan, Carl Linderholm, Dan Gall, Matthias Schmitz, Tobias Mattisson, Jan BC Pettersson, and Anders Lyngfelt. "Chemical-looping combustion in a 100 kW unit using a mixture of synthetic and natural oxygen carriers–Operational results and fate of biomass fuel alkali." *International Journal of Greenhouse Gas Control* 88 (2019): 371-382.

II. Gogolev, Ivan, Amir H. Soleimanisalim, Carl Linderholm, and Anders Lyngfelt. "Commissioning, performance benchmarking, and investigation of alkali emissions in a 10 kW_{th} solid fuel chemical looping combustion pilot." *Fuel* (2020): 119530.

III. Gogolev, Ivan, Toni Pikkarainen, Juho Kauppinen, Carl Linderholm, Britt-Marie Steenari, and Anders Lyngfelt. "Investigation of Biomass Alkali Release in a Dual Circulating Fluidized Bed Chemical Looping Combustion System." Manuscript Submitted to *Fuel (2020)*

Ivan Gogolev is the principle author of Papers I-III and conducted the experimental measurements, data processing, interpretation of results and authorship of the manuscript for papers I-III. Professor Anders Lyngfelt (who is the main academic supervisor) and Dr Carl Linderholm contributed with discussions and editing of Papers I-III. Dr Carl Linderholm also assisted in CLC pilot operation for experiments in Paper I and II. Dr. Tobias Mattisson contributed with discussions and editing of paper I. Dr. Dan Gall assisted in the setup of the instrumentation used in the experiments presented in Paper I. Professor Jan Pettersson assisted in manuscript review for Paper I. Dr Amir Soleimanisalim assisted in conducting experiments and review of the manuscript for Paper II. Toni Pikkarainen and Juho Kauppinen assisted in operating the CLC reactor in Paper III. Professor Britt-Marie Steenari assisted in reviewing the manuscript for Paper III.

Table of Contents

CHAPTER 1

1 - Introduction

1.1 Motivation

Despite the increasing awareness of global warming and over two decades of effort to combat climate change, greenhouse gas emissions in the 2000's grew faster than in the 1990's[1]. The Paris Agreement of 2015 is the latest and most extensive pledge to combat climate change. At current, 197 countries - Parties to the Paris Agreement, are committed to take action in order to limit global warming to well below 2^{o}C above the pre-industrial era average temperatures. The possible pathways to achieving this ambitious global goal were assessed by the Intergovernmental Panel for Climate Change (IPCC) and were outlined in the Fifth Assessment Report. There, 87% of the scenarios designed to meet the 2^{o}C target, heavily rely on large-scale implementation of negative emissions technologies (NETs) in the second half of this century [2]. Therefore, intensive research to support the development and implementation of NETs technologies is a crucial and pressing issue.

Many NETs technologies have been proposed in the recent years. These include direct air capture methods, reforestation and afforestation, enhanced weathering of minerals to capture CO_2 from the atmosphere, bioenergy with carbon capture and storage (BECCS), as well as many others. Although there is no clear winner amongst the current NETs technologies, BECCS is considered to be a promising lower cost option [1]. Successful, and commercially viable implementation of BECCS requires low-cost and robust fuel conversion and carbon capture technologies. Chemical looping combustion (CLC) is a novel technology that allows thermal conversion of fuels with inherent carbon capture [3]. In CLC, oxygen is delivered to the fuel by an oxygen carrier (OC) material that is circulated between two interconnected reactors. Most of the CLC schemes are based on two interconnected fluidized bed reactors, although alternative designs based on moving bed [4], packed bed [5], and rotary reactor designs [6] have been proposed. In all CLC schemes fuel conversion is accomplished by oxygen supplied with the oxygen carrier. The resulting fuel reactor flue gas

consist primarily of CO_2 and water, and is nitrogen free, thus avoiding costly gas separation. In comparative studies evaluating different carbon capture technologies, CLC has consistently been reported to have lower energy and cost penalties than competing carbon capture technologies [7–10].

CLC technology, primarily in the interconnected dual-fluidized bed configuration, has been extensively studied over the past decade. The CLC principle has been successfully demonstrated for gaseous, liquid, and solid fuels such as coal [11]. CLC of biomass, however, has not yet been extensively explored [12]. Since fluidized bed reactors are the technology of choice for biomass combustion [13], biomass should be well suited for the CLC process. In fact, the few pilot demonstrations of biomass CLC have shown promising results [14–20]. These initial investigations, however, primarily looked at short-term operation, with the reactors not extensively optimized specifically for biomass fuel operation.

Experience from contemporary biomass technologies of fluidized bed combustion (FBC) and circulating fluidized bed combustion (CFBC) shows that biomass presents significant operational challenges that stem from the high alkali content of biomass fuels. The first major issue is the onset of bed agglomeration that typically results from formation of sticky alkali-silicate melts that form within the bed material. The second detrimental issue is the deposition of alkali chlorides, alkali sulphates, and other species that form on heat exchange surfaces of the flue gas convection pass. These deposits cause fouling and corrosion of the heat exchange surfaces and result in lower thermal efficiency due to impeded heat transfer.

Like FBC and CFBC technologies, CLC reactors are expected to be challenged with alkali-induced bed agglomeration, as well as fouling and corrosion issues. Furthermore, the nature of the CLC process can introduce additional issues. The reactivity of the oxygen carrier may be affected by biomass alkali, thus having a great impact on the CLC process. The two-reactor nature of the CLC process also needs to be carefully considered. At present, it is not clear how the alkalis are released and partitioned in a CLC reactor system.

1.2 Aim and scope of this thesis

The present work aims to evaluate the implications of biomass fuel alkalis in the CLC technology context. At the inception of this work there was no published literature on the fate of alkalis in CLC. The work conducted in this thesis was focused on:

- development of a methodology to measure flue gas alkali emissions in CLC pilot systems
- establishing how biomass fuel alkalis are distributed within a CLC system
- exploring how different biomass fuels and oxygen carriers influence the release and partitioning of alkalis in a CLC system
- evaluating the implications of biomass and biomass alkalis on the operation of CLC systems

1.3 Contribution of this thesis

Paper I of the thesis, establishes the methodology for on-line measurement of alkali emissions in a CLC systems. This paper presents the first data set on fuel reactor alkali emissions in CLC systems and provides an initial insight into how alkali emissions are partitioned between the air and fuel reactors of a CLC pilot. Paper II further establishes the alkali emissions measurement methodology which is applied in a new CLC pilot system that is specifically designed for high-volatiles solids fuels such as biomass. The paper also provides a first look at the interplay between reactor performance in terms of fuel conversion and carbon capture efficiency and operational issues stemming the biomass alkali species. Paper III establishes how gas-phase alkali emissions in CLC compare to oxygen carrier aided combustion (OCAC). This paper analyses how fuel decomposition and the reactor atmosphere influence the alkali release, and how ash formation and oxygen carriers influence the retention of alkali materials in the reactor system.

1.4 Outline of this thesis

This thesis is based on the three appended papers (Papers I - III) and this introductory essay. Chapter 2 of the thesis introduces the working principle of CLC and covers background theory on alkali release in thermal conversion of biomass fuels. Chapter 3 discusses the experimental methodology and equipment used in the experiments that make up the work presented in Papers I - III. Chapter 4 explains the data acquisition, data processing, and calculation procedures used to derive the experimental findings. Chapter 5 presents and discusses the main findings of Papers I - III. Chapter 6 gives the main conclusions of the research.

CHAPTER 2

2 - Background

The following sub-sections provide the background on CLC and related phenomena. Theory of alkali release, largely from conventional combustion and gasification studies, is also explored to set the stage for extending the concepts to CLC technology.

2.1 Chemical Looping Combustion (CLC) Principle

The principle of CLC is shown in Figure 1 and consists of cyclical oxidation and reduction of a metal oxide material, the oxygen carrier (OC), circulated through two interconnected reactors.

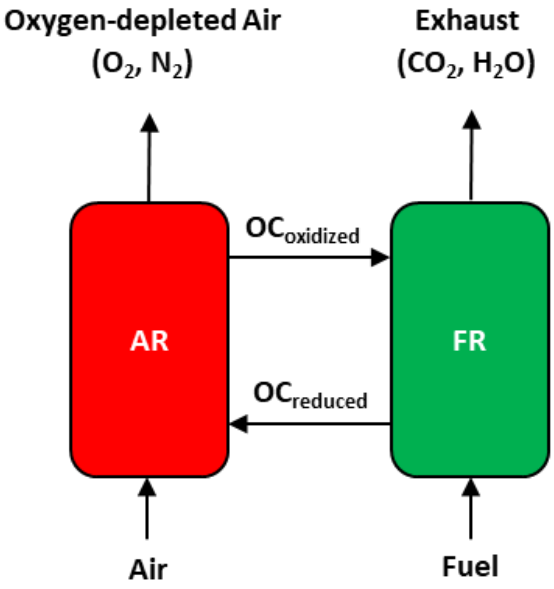

Figure 1 – Chemical looping combustion process diagram

The oxygen carrier (OC) material, typically a metal oxide, is oxidized by air in the air reactor (AR), and is reduced by the fuel in the fuel reactor (FR). In this process scheme, oxygen is

transferred by the OC from the air in the AR to the fuel in the FR, while nitrogen is rejected in the AR. Thus, fuel in the FR is converted with oxygen from the oxygen carrier, resulting in a nitrogen-free flue gas. This avoids the costly separation of CO_2 from nitrogen that is required in post-combustion CO_2 capture systems. These processes can be represented by the reactions below:

$$\text{Fuel} + a\text{Me}_x\text{O}_y \rightarrow b\text{CO}_2 + c\text{H}_2\text{0} + a\text{Me}_x\text{O}_{y-1} \quad \text{(R 1)}$$

$$a\text{Me}_x\text{O}_{y-1} + 0.5a\text{O}_2 \rightarrow a\text{Me}_x\text{O}_y \quad \text{(R 2)}$$

The OC reduction in the FR (Reaction R 1) is typically mildly endothermic, while OC oxidation (Reaction R 2) in the AR is highly exothermic. Thus, the FR is not cooled and CLC systems are designed to recover the process heat from the AR and downstream of the AR, as well as from the outgoing FR flue gas. The net heat release in a CLC system is equivalent to normal fuel combustion. The two-reactor scheme essentially separates the combustion reaction into two separate steps; each involves the OC and occurs in a separate reactor. The CLC process is most typically implemented in a dual-fluidized bed arrangement. Description of such systems is covered in Chapter 3 of this thesis.

2.2 Chemical Looping Combustion Fuels

Gaseous Fuels

CLC was initially developed and demonstrated with gaseous fuels [3]. Gaseous fuel, typically methane or syngas, is introduced at the bottom of the fuel reactor as the fluidizing gas. As the fuel gas makes its way through the OC bed, it reacts with the solid oxygen carrier and is converted to CO_2 and H_2O. Fuel conversion of gaseous fuels in CLC is typically quite high and can reach nearly 100% with highly reactive oxygen carriers such as nickel [21]. Fuel conversion primarily relies on the properties of the oxygen carrier and contact between the fuel and the oxygen carrier. As such, the fluidization regime and bed height have a significant impact on fuel conversion.

Solid Fuels

For solid fuels, the fuel conversion process is more complex and involves in-situ gasification of the fuel char. The OC bed of the FR is typically fluidized by CO_2 or steam, with the solid fuel fed directly into the bottom section of the reactor bed by means of a screw-feeder or

pneumatic transport. As the fuel enters the rector bed, it is rapidly heated and undergoes the following staged decomposition:

1. Drying – water content is removed by evaporation from the fuel particles
2. Devolatilization – the fuel's volatile contents are released in the vapor phase, leaving behind solid char and most of the inorganic fuel content
3. Gasification – char is gasified by reacting with the CO_2 or steam fluidizing medium, leaving behind fuel ash. The main gasification reactions are [22]:

$$C_{(s)} + H_2O_{(g)} \rightarrow CO_{(g)} + H_{2(g)} \quad \text{(R 3)}$$

$$CO_{(g)} + H_2O_{(g)} \rightarrow CO_{2(g)} + H_{2(g)} \quad \text{(R 4)}$$

$$C_{(s)} + CO_{2(g)} \rightarrow 2CO_{(g)} \quad \text{(R 5)}$$

4. Oxidation – volatiles released in devolatilization, as well as the char gasification products, are oxidized by reacting with the oxygen carrier material, as per reaction R1.

Of these process steps, steps 1 through 3 are sequential, but step 4 occurs concurrently with the others. A simplified visualization of the staged decomposition process is presented in Figure 2.

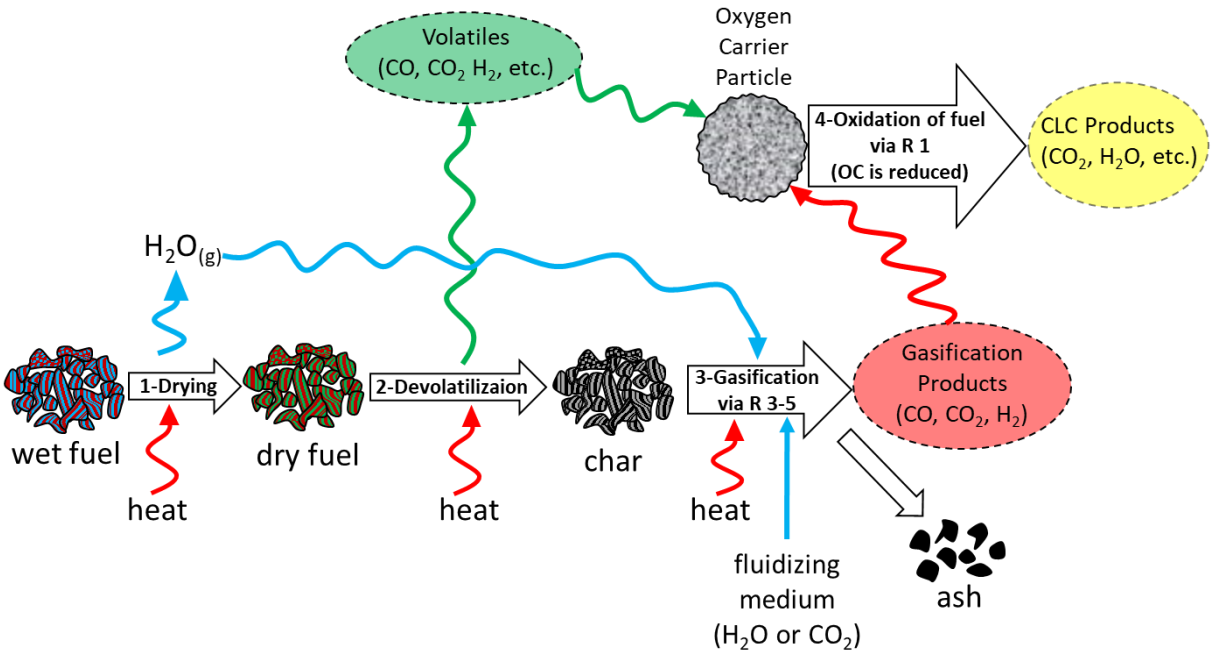

Figure 2 – Solid fuel conversion in chemical looping combustion

Solid fuel use in CLC presents challenges that arise largely from the fuel's composition. Typical composition ranges of several solid fuels are presented in the Table 1.

Table 1 – Proximate analysis of selected solid fuels from Phyllis 2 database[23]

	Fossil Fuels			Biomass Fuels		
Property	**Lignite Coal**	**Petroleum Coke**	**Finnish Peat**	**Pine Sawdust**	**Wheat Straw**	**Rice Husk**
Moisture content (wt% a.r.)	13.40	0.32	9.80	13.67	15.10	11.20
Ash content (wt% a.r.)	3.32	0.40	6.77	1.15	7.60	18.29
Volatile matter (wt% a.r.)	42.61	17.24	65.49	69.45	62.32	48.31
Fixed carbon (wt% a.r.)	40.68	82.04	17.95	15.73	14.98	22.20
Lower heating value (MJ/kg)	20.15	36.10	20.70	16.46	13.60	10.70

For fossil fuels, such as coal and coke, the relatively high fixed carbon content presents a challenge. For such fuels, char gasification is often the slowest and rate limiting step of the thermal conversion sequence outlined above [12,22]. Slow gasification can cause unconverted char elutriation into the FR's flue-gas stream, or carryover of char from the FR to the AR. Char elutriation in the FR causes incomplete fuel conversion and can overwhelm the downstream flue-gas clean-up system. In larger pilot scale studies with fuels such as coal and petroleum coke, elutriated fuel fractions were reported to range from 5% to 50%, depending greatly on the fuel type, fuel size, fuel residence time, oxygen carrier material, and other operating parameters [12]. Char carryover to the AR leads to char combustion, and consequentially the release of uncaptured CO_2 from the AR. To mitigate such undesirable effects several reactors have been designed to have either a dedicated or integrated carbon stripper section in the FR. Both approaches rely on elutriating the char from the OC and reintroducing it back to the FR, thus giving the char more time convert and gasify.

Biomass Solid Fuels

Biomass conversion in CLC differs from that of other solid fuels. Biomass has a much higher volatile content than that of solid fossil fuels such as coal and coke. Depending on the type, biomass volatiles content is typically in the range of 63-85 wt% on dry fuel basis, while coals typically contain 18-43 wt% [13,24]. Due to the high volatile content, on average, approximately 50-75% of the biomass fuel's mass is released in the devolatilization stage [24]. While this may not be an issue in conventional fluidized-bed combustion where biomass burns in the reactor bed and freeboard in the presence of excess air, in CLC, combustion of the released volatile species depends on effective contact with the oxygen carrier material. Depending on where the volatiles are released, their conversion can vary. Volatiles released at the bottom of the FR have a greater chance of achieving full oxidation as they make their way up through the OC bed. Volatiles released in the top portion of the bed have a lot less time for contact [22]. Although higher OC inventory or lower fuel feeding rate can improve contact between the released volatiles and the OC material, in practice, full oxidation of the volatiles typically does not occur. Achieving full conversion requires downstream injection of pure oxygen in order to complete the oxidation. This oxygen injection step is often termed "oxy-polishing" [12]. For similar operating conditions, fuels with higher volatile content tend

to require more supplemental oxygen to complete the oxidation of the produced gaseous species [12].

Biomass char conversion is also different from other solid fuels. Biomass contains less fixed carbon and therefore produces less char [24]. Biomass char is also more reactive than that of fossil fuels due to several factors. Biomass char tends to be more porous, with larger pore sizes. This increases the char's reactivity due to higher active surface area and improved diffusion [13]. Further, and perhaps more significantly, biomass tends to contain a significantly higher levels of alkali (K and Na), compared to fossil-based solid fuels. Alkalis act as catalysts for char gasification, thus increasing the rate of char conversion [13,25,26].

2.3 Oxygen Carriers

Oxygen carrier materials constitute the cornerstone of chemical looping combustion technology. Selection of an oxygen carrier is quite complex and is highly dependent on the application. Nevertheless, the following parameters are considered critical:

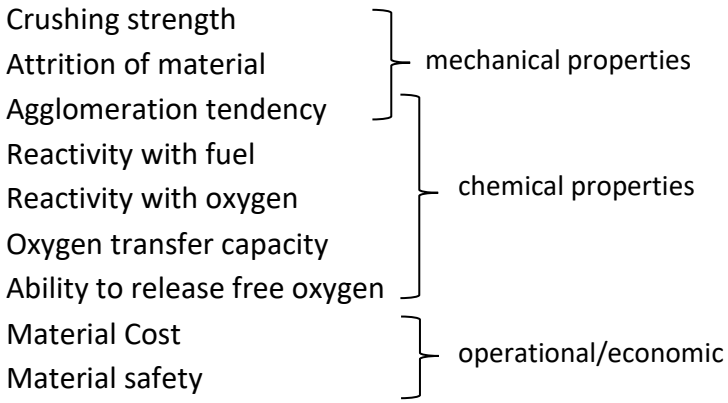

Over 1000 potential OC materials have been investigated to date [27]. At the highest level, these materials can be divided into high-performing manufactured materials, and the less effective low-cost materials.

Manufactured Materials

Manufactured oxygen carriers are typically based on oxides of Ni, Fe, Mn and Cu supported on inert materials such as Al_2O_3. These materials were primarily developed for CLC of gaseous fuels and optimized for high conversion of CH_4. Further to single oxide oxygen carriers, multiple mixed-oxide and combined-oxide oxygen carriers have been successfully developed for CLC. Mixed-oxide oxygen carriers are based on physical combination of different metal oxides in one oxygen carrier material. Combined oxide oxygen carrier materials are made by chemically combining two or more metal oxides or by forming materials with a perovskite structure. The advantage of these manufactured materials is that their properties can be

tailored, but the major disadvantage is their high cost. Due to high cost, manufactured oxygen carriers are primarily suited for use with gaseous fuels, where the oxygen carrier lifetime in the CLC system can justify the investment. Use of manufactured oxygen carriers with solid fuels is cost prohibitive, as solid fuel CLC is often accompanied with significant ash formation. Ash formation can contaminate or deactivate oxygen carriers and limit their useful lifetime [27].

Low-Cost Materials

Low cost oxygen carriers are materials which have oxygen carrying properties but are either naturally occurring (such as manganese ore, iron ore, and ilmenite), or are low-cost industrial by-products (such as steel slag). In all cases, these materials contain naturally occurring metal oxides, along with other inorganic matter that exhibits oxygen carrying behavior. The major disadvantage of such materials is that their properties are set, and their reactivity towards methane is generally quite low. This makes most low-cost oxygen carriers a poor choice for CLC with gaseous fuel. However, the reactivity of these same materials with CO and H_2 is generally much higher. Since solid fuel conversion invariably relies on gasification of char to CO and H_2, low-cost materials can be sufficiently reactive with solid fuels [28,29]. The low cost of these materials, when compared to manufactured oxygen carriers, also makes them the only economically justifiable choice for CLC with solid fuels, where effects of fuel ash can greatly limit the oxygen carrier's useful lifetime. Ilmenite, a naturally occurring titanium-iron oxide ($FeTiO_3$) is by far the most widely used low-cost material which has been extensively and successfully used in CLC operation with solid fuels [12].

Oxygen Carriers for Chemical Looping with Oxygen Uncoupling (CLOU)

Some oxygen carrier materials have the ability release molecular oxygen in conditions typical of the FR. Chemical looping combustion operation with such oxygen carriers is a subset of CLC technology, called chemical looping with oxygen uncoupling (CLOU) [30]. Three metal oxide systems that show oxygen release appropriate for the CLOU process are the Mn_2O_3/Mn_3O_4, CuO/CuO_2 and CoO_4/CoO systems. These oxide systems have been used to create manufactured CLOU oxygen carriers, but are also present in some naturally occurring materials. For example, several manganese ores exhibit CLOU behavior [31–33]. In the CLOU process, gaseous oxygen is released from the OC in the FR. This enables the fuel to be directly oxidized by the free oxygen, instead of reacting with the solid oxygen carrier. Although useful for all fuel types, the CLOU process is especially beneficial for solid fuel conversion. Whereas in non-CLOU CLC, char conversion is often rate-limited by the slow gasification step, in the CLOU process, char can be converted directly to combustion products by reacting with the free oxygen released by the oxygen carrier. The CLOU process essentially partially eliminates the slow char gasification step [12,16]. Experimental studies have shown that CLOU is able to accelerate the rate of fuel conversion by a factor of 45 for petroleum coke and by a factor of 60 for bituminous coal, when compared to the conversion rates of these fuels in a non-CLOU

CLC process [17]. The improved fuel reactivity observed in the CLOU process also realizes the benefit of a much-reduced OC inventory [17]. This is because in non-CLOU operation, gaseous fuel components (the volatile fuel fraction and the gasification products) require adequate contact time with the OC to reach a reasonable conversion level. This is typically achieved by increasing bed material height, and thus inventory levels. In the CLOU process, the gaseous fuel components react in contact with the OC (gas-solid reaction) but have the additional benefit of reacting with the molecular oxygen released by the CLOU oxygen carrier. Contact of the free oxygen with the gaseous fuel fraction is much more efficient, and thus, less OC inventory is required. In fact, conversion of volatiles by free molecular oxygen can occur above the bed of the fuel reactor.

2.4 Alkali-Related Issues in Thermal Conversion of Biomass

In conventional thermal fuel conversion processes of combustion and gasification, biomass fuels are known to cause issues that stem from their inorganic fraction. Biomass inorganic content can vary greatly from <1 wt% for woody biomass to as high as 40 wt% for green house residues. The inorganic (ash) content of several selected fuels is shown in Table 1. Ash analysis showing distribution of inorganic species for several biomass fuels and a fossil fuel is presented in Table 2, as reproduced from reference [34].

Table 2 – Ash composition for selected biomass and fossil fuels [34]

Fuel	SiO_2	Al_2O_3	Fe_2O_3	Mn	MgO	CaO	Na_2O	K_2O	TiO_2	P_2O_5	SO_3
Wood pellets	4.3	1.3	1.5	5.9	8.5	55.9	0.6	16.8	0.1	3.9	1.3
Demolition wood pellets	20.4	3.5	2.2	0.3	7.5	27.5	4.8	10.5	2.5	11.1	LLD
Pepper plant residue	12.6	4.9	2	0.2	7.4	32.2	0.9	24.6	0.5	5.2	LLD
Greenhouse residue	28.4	3.9	18.4	0.3	5.7	25.8	0.8	9.7	0.8	3.8	LLD
Sunflower pellets	2.9	0.6	0.8	0.1	21.6	21.6	0.24	22.8	0.1	15.2	14
Olive cake pellets	12.8	2.9	3	0.1	4.9	17.5	3.9	47.9	0.2	6	1.1
Wheat straw	53.1	3.6	1.2	N.R	3	17.7	4.5	30	N.R	4.1	N.R
Sewage sludge	38.3	0.8	12.5	N.R	2.8	9.1	2.2	2.2	0.8	15.4	1.1
Bituminous Coal	59.7	20.3	7	< 0.01	1.9	1.8	1	2.3	0.9	0.1	1.3

From the common inorganic species presented in oxide form in Table 2, some are relatively benign and do not cause significant issues in combustion and gasification. However, K and Na alkali species, along with Cl, are considered highly problematic, as their release is associated with severe operational issues. In the bed material of fluidized bed boilers and gasifiers, alkali species are known to be responsible for causing bed material agglomeration [24,34,35] . When released to the flue gas, alkali species are known to cause fouling and corrosion of heat exchange equipment [34,36,37].

Alkali Release and Retention in Biomass Thermal Conversion

K and Na are present in biomass in three primary forms: 1) salts, 2) organically associated form, and 3) excluded minerals. Alkali species present as excluded minerals arise mostly from

contamination of fuel during fuel preparation and processing. In combustion processes this form of alkali species tends to be quite inert and does not have significant implications for thermal conversion [36]. Alkali salts and organically associated alkalis, however, are known to be releasable and reactive during the fuel conversion process. From these forms, alkalis present in salt form are estimated to account for up to 90% of the biomass alkalis [38,39]. The release and reactivity behavior of K and Na is considered to be equivalent [36]. For this reason, and because the abundance of K in biomass far exceeds that of Na, further discussion is based on release and transformations of the K species. The transformations discussed below are equivalent for Na.

Alkali species are released in different proportions during thermal conversion of biomass. As biomass fuel is introduced into a reacting system (e.g. boiler, gasifier), it is heated and undergoes a staged decomposition process. As the fuel particle temperature rises, devolatilization starts to occur. This step is common to combustion and gasification processes. At the devolatilization stage about <10% of K is released at temperatures below 700^{o}C [38,40]. Since the K release in the devolatilization step is quite small, most of the K species remain trapped in the char fraction as char-bound K, as K salts such as K_2CO_3 and K_2SO_4 and as silicates [40].

Further fuel decomposition differs for combustion and gasification. In combustion, char is oxidized to CO_2, while in gasification the char if gasified to CO and H_2. In both processes, the high temperature release occurs >700^{o}C and is dominated by evaporation of KCl to the gas phase. The amount of KCl fraction in the char depends on the original fuel, with annual biomass typically containing more KCl, and on release of Cl. Several studies estimate that up to 75% of the fuel's Cl can be released at lower temperatures in the devolatilization stage through formation of $HCl_{(g)}$ [38,41]. After KCl evaporation, further release of K occurs through devolatilization of char bound K and decomposition of K_2CO_3 and K_2SO_4.

Throughout the fuel conversion process gas phase release of K is counteracted by competing formation of K-silicates. At high temperatures K readily reacts with SiO_2 and Al to form potassium silicate or aluminosilicate species [40]. Silicate species remain in condensed form at temperatures below 1200^{o}C, but start to decompose releasing K to the gas phase at higher temperatures [38]. Both, the release and retention of K, can have detrimental effects on the thermal conversion system's operation.

Implications of Gaseous Alkali Release

Alkali species released to the gas-phase are known to cause fouling and corrosion of heat exchange equipment in contact with the flue gases. In boilers used for steam production, steam superheaters are operated at temperatures of approximately 400-600^{o}C, while typical combustion temperatures are maintained in the range of 800-900^{o}C. Deposition of gaseous alkali species occurs as the flue gas begins to cool in the vicinity of the heat exchangers. Alkali salts condense onto the surface of the heat exchanger, forming a sticky coating. Further

deposition occurs via further condensation of gaseous alkali species or by impaction of fly ash and other condensed species [37]. The formed deposits insulate the steam tubes and impede heat transfer, leading to lower overall heat extraction and consequently lower boiler thermal efficiency. Extreme deposit growth requires installation of soot blowers that are used to clean the deposits off the steam tubes without having to take the boiler offline. Soot blower equipment, however, is costly to install and operate. Depending on the species present in the deposits, severe corrosion of steam tube materials can occur. Of the possible species, KCl is known to be especially detrimental as it causes severe high temperature corrosion [23]. In extreme cases corrosion permanently damages the steam tube material, requiring boiler shutdown to replace the compromised tube packs. KCl-induced corrosion is typically dealt with by addition of sulfur (S) to the fuel. In the boiler, S reacts with KCl to form K_2SO_4 and HCl. Although these species also participate in corrosion, they are significantly less aggressive than KCl. Sulfur is typically added to the process by co-firing with sulfur-containing fuel (e.g. sewage sludge), addition of elemental sulfur, or addition of sulfur containing species (e.g. ammonium sulfate) to the flue gas of the boiler.

Implications of Alkali Retention

Alkali species that are trapped within the bottom ash fraction can also be problematic for boiler or gasifier operation. Alkali silicate species that form by reaction of alkalis with SiO_2 have a melting point of approximately 700^{o}C [23]. Since typical biomass-fueled furnaces operate at around 800-900^{o}C, alkali silicates form sticky melts. Once significant amounts of these melts are formed, the bed material particles start to stick together and form agglomerates. With continued operation, severe agglomeration of the bed material leads to defluidization and shut down of the process units [24,34,35]. Agglomeration can be dealt with, to some extent, by reducing combustion temperatures to limit the formation of the sticky melts. This strategy, however, results in inefficient combustion. In practice, mitigating or limiting agglomeration is managed by continuous replacement of bed material (i.e. removal of old material with makeup of fresh material). Large scale commercial boilers operated with agglomeration-prone fuels can require continuous material replacement of up to 1/3rd of the boiler inventory per day of operation [22]. Other methods to mitigate agglomeration involve adding aluminum containing materials such as kaolin, or other clay minerals. Aluminum readily reacts with alkali silicates to reform them to aluminosilicates that have a much higher melting point. Another strategy involves using alternative bed materials such as olivine, dolomite, blast furnace slag, feldspar and others [42].

2.5 Alkalis in CLC

At the onset of the work presented in this thesis, the fate of alkalis in CLC was largely unexplored, with only several pilot-scale studies reporting qualitative observations on the interaction of alkalis with OC materials. Gu et al. reported alkali deposit formation on the surface of the iron ore OC in 1 kW CLC operation with wood sawdust fuel. In this study, the

alkali deposit was found to have no effect on the oxygen carrier reactivity [43]. In a similar investigation at 500 W scale, Mendiara et al. found no alkali deposition or alkali effect on reactivity of iron ore OC [17]. Other results on alkali interaction with oxygen carriers were reported from studies using ilmenite oxygen carrier in oxygen carrier aided combustion (OCAC) [44] and in gasification [45]. Both studies showed that that ilmenite can capture potassium. This property was attributed to ilmenite's TiO_2 fraction that can form stable potassium titanate compounds within the ilmenite OC particles. The few reported interaction results made it clear that alkalis can affect the OC, and in turn, the OC can influence alkali behavior. Thus OC-alkali interactions should be carefully considered when evaluating oxygen carrier materials for use in CLC of biomass.

How alkalis are released and partitioned within a CLC system operated with biomass was untested prior to the studies presented in Papers I through III. However, considering the nature of the CLC process led to the expectation that in CLC most of the alkali release to the gas phase should occur in the fuel reactor. This expectation was based on the knowledge that alkali release in thermal conversion is known to occur during fuel decomposition, and the fact that fuel decomposition occurs primarily in the FR. Beyond this hypothesis and the few interaction observations, the nature of alkali in CLC was and still is an uncharted territory that poses the following main research questions:

1. Where and how are alkalis released to the gas phase in CLC?
2. Where and how are alkalis retained in a CLC system?
3. How do alkalis influence OC reactivity and CLC performance?
4. How do OC materials influence ash formation and related issues?
5. How does alkali behavior in CLC differ from conventional combustion?
6. Does the CLC process hold any advantage or disadvantage for thermal conversion of biomass fuels?

The work presented in this thesis attempted to start answering at least a few of the posed questions.

CHAPTER 3

3 - Experimental Setup

The work presented in this thesis is based on three experimental campaigns conducted in three different CLC pilot systems. The following sections provide an overview of the CLC pilots, the oxygen carriers and fuels, and the alkali measurement system used in the campaigns.

3.1 CLC Pilot Systems

Three different CLC pilot reactor systems were used in the experimental work presented in this thesis. Schematics for these systems are presented in Figures 3 to 5. The key features of the reactors are summarized in Table 3.

Table 3 – Key features of the CLC pilots used in the experimental investigations

CLC Pilot	**Nominal Duty**	**System Inventory**	**AR Configuration**	**FR Configuration**	**Reactor Connections**	**Special Features**	**Heating**
100 kW (Chalmers) **Paper I**	100 kW	150-250 kg	High velocity riser with cyclone	CFB	Loop Seals	Circulation riser, carbon stripper	Oven
10 kW (Chalmers) **Paper II**	10 kW	25-40 kg	High velocity riser with cyclone	Bubbling fluidized bed	Loop Seals	Volatiles distributor	Oven
D-CFB (VTT, Finland) **Paper III**	60 kW	50-60 kg	CFB	CFB	L-valves		Wall heat tracing

100 kW Solid Fuels CLC Pilot (Chalmers)

The 100 kW CLC pilot shown in Figure 3 was used in experiments presented in Paper I. The fuel reactor in this system has a circulating fluidized bed (CFB) design with a 5 m tall main riser. The oxygen carrier travels through the FR's main riser section and is then returned to the bottom of the FR riser via a cyclone (CY2) and a loop seal (LS2). This design allows for control of internal FR material circulation and improved contact between the fuel's gaseous components and the OC material. Material from the FR eventually overflows and travels by gravity to the circulation riser (CR) via a loop seal (LS3). The CR transports the OC material to the carbon stripper (CS), where residual unconverted char particles are gasified or elutriated, and recirculated back to the FR. From the CS, the OC material is gravity-fed to the AR via a loop seal (LS4). In the AR, the OC is oxidized and transported back to the FR via a cyclone (CY1) and loop seal (LS1). The CR is implemented to make the system more compact. Without the circulation riser, the overall height of the system would be several meters taller, since the OC needs to be gravity-fed from the FR to the carbon stripper (CS), and from the CS to the AR. Solid fuel is fed into the system with a screw feeder (not shown) to the top of the LS2 loop seal. The entire reactor system is located in an electrically heated oven that maintains the reactor temperature. Excess heat from the AR is removed with a mantle cooler that uses ambient air as the heat transport medium. The 100 kW reactor system is described in more detail in a study by Markström et al. [46].

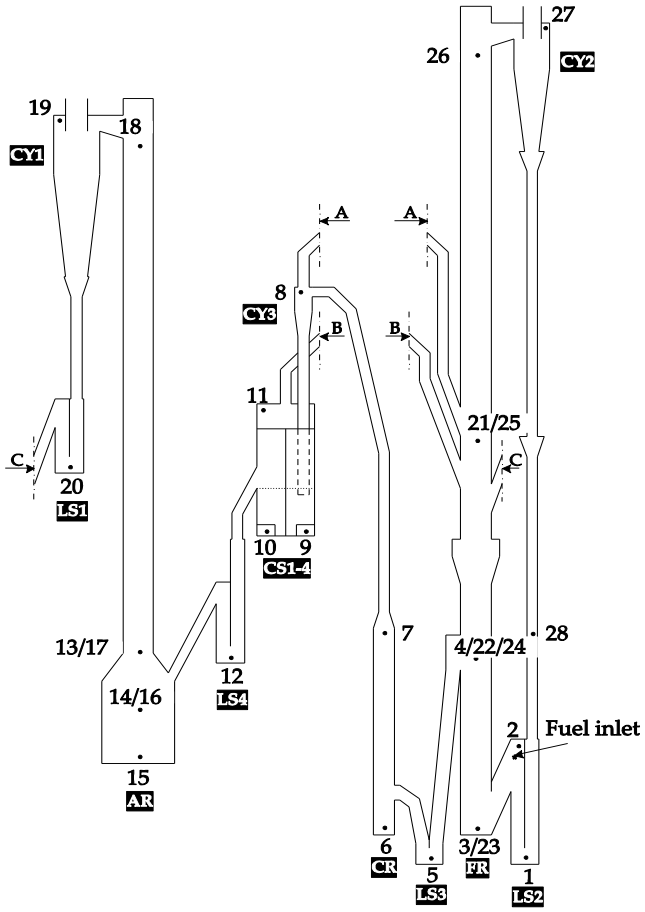

Figure 3 – 100 kW CLC pilot for solid fuels

10 kW Solid Fuels CLC pilot (Chalmers)

The 10 kW CLC pilot shown in Figure 4 is a newly designed and built CLC pilot system that was commissioned with the experiments presented in Paper II. This pilot system consists of a high velocity riser AR, and a bubbling fluidized bed FR. OC particles from the FR are fed by gravity to the AR via the lower loop seal (LLS). Oxidized OC particles are transported from the AR to the FR up the AR riser via the AR cyclone and the upper loop seal (ULS). Solid fuel is gravity-fed into the FR with from a fuel hopper. The reactor is installed in an electrically heated oven that maintains the reactor temperature. The bubbling fluidized bed FR was specially designed for operation with high volatiles solid fuels such as biomass. The FR internals include a volatiles distributor, which is essentially a perforated internal baffle. The volatiles distributor is meant to help in contacting the fuel volatiles with the bed material by forcing the released volatiles through small gas distribution holes. A more detailed description of this pilot system, the details of the volatiles distributor, as well as description of the auxiliary equipment (fuel feeding system, flue gas filtration) can be found in Paper II.

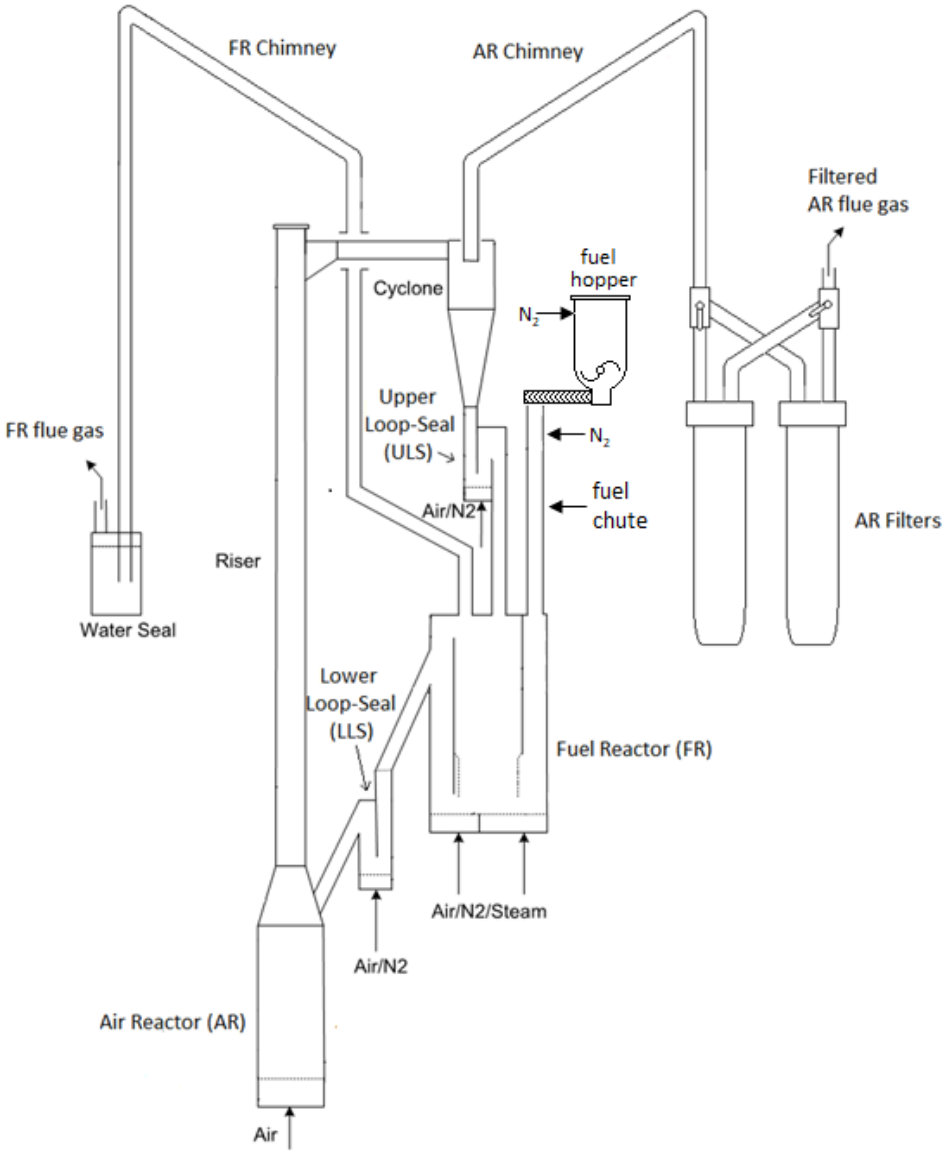

Figure 4 – Simplified schematic of the new 10 kW solid fuels CLC system

Dual Circulating Fluidized Bed (D-CFB) CLC pilot (VTT, Finland)

The dual circulating fluidized bed (D-CFB) CLC pilot shown in Figure 5 was used in experiments presented in Paper III. This system is located at the VVT research institute's Bioruukki piloting center in Espoo, Finland. In this system, both the FR and AR, have a circulating fluidized bed (CFB) design. OC material from the FR is transported up the FR riser and is gravity-fed to the AR via the FR cyclone and the return leg which connects the bottom of the FR cyclone to the bottom of the AR. The oxidized OC material is transported up the AR riser and is gravity-fed to the bottom of the FR riser via the FR cyclone and a return leg. The AR and FR return legs act as L-valves and use nitrogen fluidization to avoid gas mixing between the AR and the FR. The D-CFB pilot is equipped with capability to feed solid fuels to both, the AR and the FR, from two independent solid fuel feeding systems. Unlike the 100 kW and 10 kW CLC pilots described above, the D-CFB pilot is heated with electrical heat tracing which is installed locally on each reactor section. This results in higher temperature difference between the AR and FR. A more detailed description of this system is provided in Paper III.

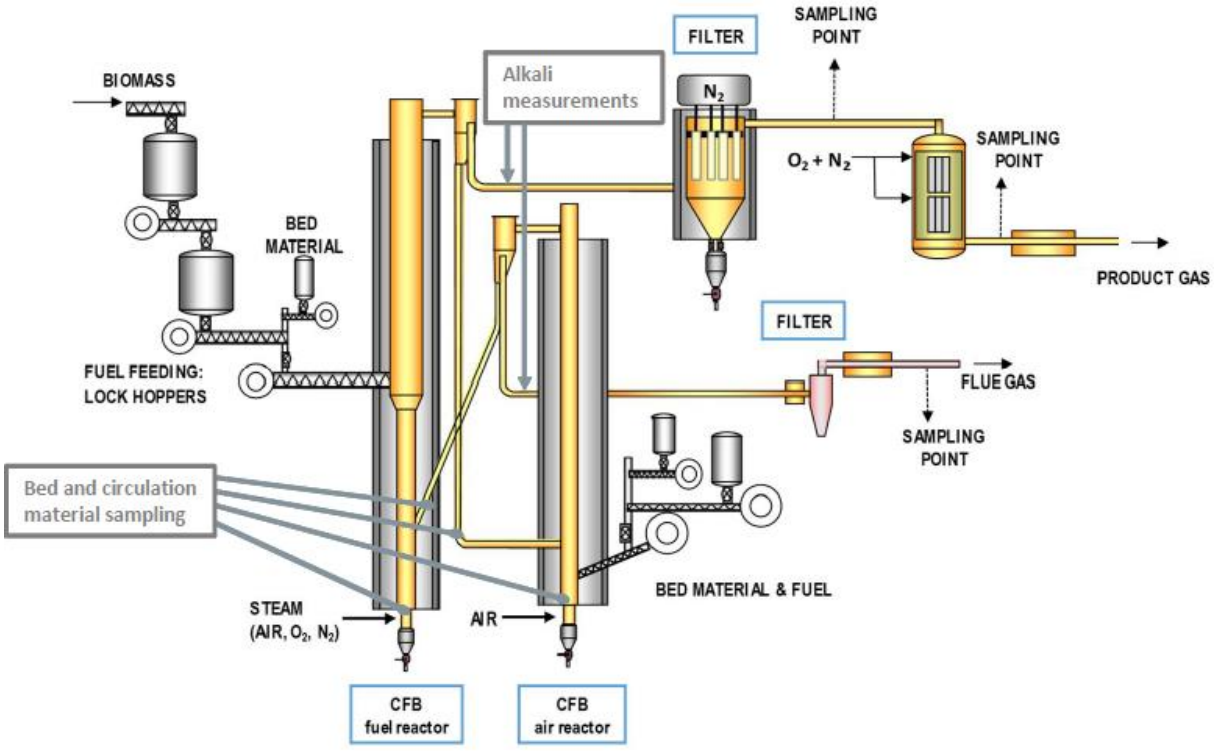

Figure 5 – Schematic of the D-FBC CLC pilot (VTT, Finland)

3.2 Fuels and Oxygen Carriers

The oxygen carrier materials used in experiments presented in Papers I through III are summarized in Table 4.

Table 4 – Oxygen carrier materials, Papers I-III

	Oxygen Carrier	Chemical Formula	Material Origin	CLOU effect
Paper I	Ilmenite + Calcium Manganite	$FeTiO_3$ + $CaMn_{0.775}Ti_{0.125}Mg_{0.1}O_{3-\delta}$	Fe-Ti ore + synthetic perovskite	No Yes
Paper II	Ilmenite	$FeTiO_3$	Fe-Ti ore	No
Paper III	Ilmenite	$FeTiO_3$	Fe-Ti ore	No
	Braunite	Mn_7SiO_{12}	Mn ore	Yes

Note: δ is the perovskite structure oxygen deficiency factor

In Table 4, calcium manganite is a synthetic perovskite material with its elemental composition defined by its chemical formula. This material was mixed with ilmenite in different proportions throughout the experimental campaign in Paper I (see Paper I for details). For ilmenite and braunite the chemical formula represents the ore's main component. The actual elemental composition of ilmenite and braunite is presented in Table 5.

Table 5 – Elemental composition of ilmenite and braunite oxygen carriers

Element	Unit	Ilmenite	Braunite
Ti	wt%	27.36	0.020
P	wt%	0.004	0.030
S	wt%	0.026	0.13
Cr	wt%	0.051	0.010
Fe	wt%	35.89	11.0
Si	wt%	0.76	2.50
V	wt%	0.11	<0.01
Ca	wt%	0.15	3.50
Mg	wt%	2.23	0.89
Al	wt%	0.34	0.25
Mn	wt%	0.23	55.0
K	wt%	0.017	0.020
Na	wt%	0.052	0.22
Zn	wt%	0.012	0.010
Ni	wt%	0.018	0.010
Cu	wt%	0.007	0.040
Co	wt%	0.012	0.020
Sr	wt%	0.003	0.12
Zr	wt%	0.017	0.020
Nb	wt%	0.005	<0.0001
Pb	wt%	<0.0001	0.010
Cl	wt%	<0.01	0.030
O (remainder)	wt%	32.7	26.2

The fuels used in the experiments of Papers I through III are presented in Table 6 along with the fuels' composition and heating values.

Table 6 – Biomass fuel composition

Parameter	Unit	Black Pellets (BP)	Swedish Wood Char (SWC)	Swedish Wood Char (SWC)	Pine Forest Residues (PFR)	Straw Pellet Mix (SPM)	Wood Pellets (WP)	Wood Char (WC)	Straw Pellets (SP)
Moisture	wt% a.r.	6.90	3.90	5.10	9.20	7.85	7.50	4.10	8.10
Ash	wt% a.r.	0.279	5.50	2.80	1.82	4.09	0.460	14.0	5.51
Volatiles	wt% a.r.	74.2	16.7	15.7	80.0	74.6	78.4	18.7	69.3
Fixed Carbon	wt% a.r.	18.7	73.9	76.4	9.0	13.5	13.7	63.2	17.1
H	wt% a.r.	5.59	3.30	3.00	5.69	5.84	5.64	2.21	5.24
C	wt% a.r.	49.8	78.7	81.2	46.9	45.9	46.9	73.0	43.2
N	wt% a.r.	0.093	0.360	0.480	0.347	0.377	0.160	0.960	0.580
O	wt% a.r.	37.4	12.1	12.5	36.0	40.2	39.4	5.75	37.2
K	mg/kg fuel a.r.	460	2585	4400	2080	5730	202	1560	6870
Na	mg/kg fuel a.r.	<53	<270	<110	27	157	122	114	61.0
Cl	mg/kg fuel a.r.	<100	<100	-	-	1700	26.0	101	3320
S	mg/kg fuel a.r.	<120	<300	180	400	1080	93.0	288	1010
Si	mg/kg fuel a.r.	<530	2060	12000	-	9770	88.0	378	9210
Ca	mg/kg fuel a.r.	820	5900	12000	-	4260	994	47000	3360
LHV	MJ/kg a.r.	18.6	29.8	30.0	18.0	16.8	17.3	26.1	15.8

3.3 Reactor Gas Analysis

All three CLC pilot systems described above were equipped with online gas analyzers to measure the gas composition of the AR and FR flue gases. The gas analysis systems for each reactor consists of a gas conditioning system and a gas analyzer. The gas conditioning system condenses the moisture from the sampled gas, so water does not affect the analyzer operation. FR flue gas sampling on the 100 kW and 10 kW CLC pilots also includes additional filtration and condensers which clean the sampled gas from particles and excess water. The FR flue gas analyzers measure concentration of CO_2, CO, CH_4, H2 and O_2, while the AR flue gas analyzers measure CO_2, CO and O_2 concentration. Gas analysis of the flue gas is the key process measurement that allows for calculating critical operation performance parameters of carbon capture efficiency and gas conversion efficiency. More details on the gas analysis (analyzer model, measurement principle, measurement range, uncertainty, sampling rates) are provided in Papers I through III.

3.4 Alkali Measurement System

There are several methods for measuring gas-phase alkali emissions. Offline measurement methods include gravimetric sampling of condensed alkali particles with impactors or filters, followed with subsequent ex situ analyses of the collected particles. These methods are useful for speciation of the collected alkali but can only quantify average emissions over extended measurement periods. Online methods include optical-based methods such as excimer laser induced fragmentation fluorescence (ELIF) [47], tunable diode laser absorption spectroscopy (TDLAS) [48], inductively-coupled plasma optical emission spectroscopy (ICP-OES) [49], molecular beam mass spectroscopy (MBMS) [50] and thermal methods such as volatility

tandem mobility analysis (VTDMA) [51]. ELIF and TDLAS are in situ techniques and are not suitable for alkali measurements in CLC since the AR and FR flue gas streams are typically laden with oxygen carrier fines. The ICP-EOS technique is extractive but is complex and impractical for implementation in a CLC pilot. The VTDMA technique is also extractive but is complex and relies on lengthy stable operation periods which are difficult to maintain in experimental CLC campaigns.

The surface ionization detector (SID) is another online extractive alkali measurement technology that has been successfully implemented for alkali emission measurements in bench-scale experiments [27,28] and industrial scale investigations [8,20,29]. Experience from these studies shows that the SID technique is relatively easy to implement and allows for sensitive measurement of total alkali species that contain K and Na [39]. For these reasons the SID technology was chosen for the investigations presented in Papers I through III. The following subsections provide details on the SID's operating principle and explain how the SID was implemented in the experimental CLC campaigns covered in this thesis.

Surface Ionization Detector Instrument

The SID implemented in the experiments covered in this thesis was developed based on previously implemented SID designs [26] but includes several modifications. A simplified diagram of the SID is presented in Figure 6.

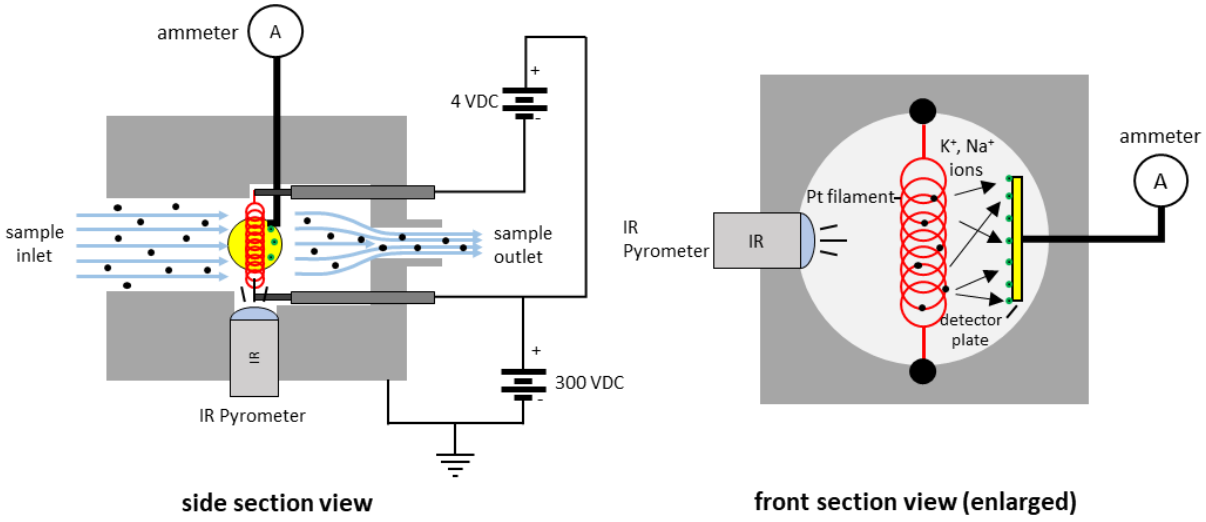

Figure 6 – Surface ionization detector (SID) diagram

The SID implemented in this work is a straight path flow-through device. The sample flow path is cylindrical with an inner diameter of 25 mm. A 0.2 mm diameter platinum filament formed into a loose coil is installed in the flow path of the sample. This filament is resistively heated and biased with +300 VDC. A metal detector plate is installed adjacent to the coil and is connected to highly sensitive ammeter capable of measuring current down to the picoampere level. An infrared pyrometer is installed opposite the coil for monitoring of the filament temperature.

In operation, gas containing condensed alkali aerosol flows through the SID, passing by the Pt filament. The sample flow is drawn by a pump at the outlet of the SID instrument. The flow is controlled by an electronic mass flow controller (MFC) at 0.5 nL/min. The Pt filament is maintained at 1100°C with the temperature monitored by the IR pyrometer. Flowing alkali particles in the vicinity of the hot filament melt on the surface of the platinum. Surface ionization on platinum selectively ionizes K^+ and Na^+ cations, which are then pushed away from the Pt filament due to its 300 VDC positive bias. K^+ and Na^+ ions that impact the collector plate induce a current which is measured by the ammeter. The current measured by the ammeter can be directly correlated to the alkali concentration in the sample. The SID is capable of detecting alkalis in condensed and gaseous form. However, direct sampling of flue gas (typically at 900°C or more), results in uncontrolled condensation of alkali onto the walls of the sampling lines that leads to the SID instrument. To minimize such losses, the sample drawn from the flue gas has to be conditioned to induce controlled nucleation of alkali in the sample flow. The setup of the SID-based alkali measurement system for use in CLC underwent significant and progressive development from the implementation used in Paper I to later experiments in Papers II and III.

SID Alkali Measurement System

A schematic of the entire SID-based alkali measurement system is shown in Figure 7. This system consists of three main sub-systems: the sampling and dilution system, the SID instrument, and the calibration system.

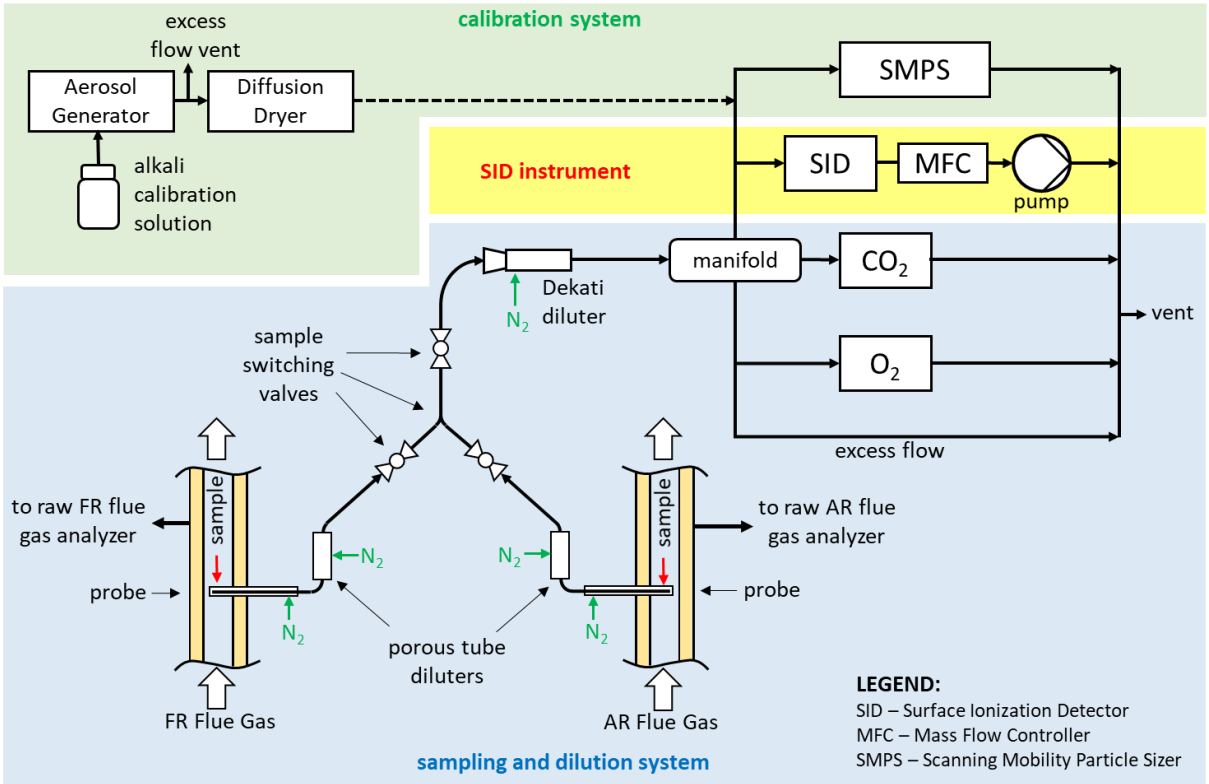

Figure 7 – SID alkali measurement system simplified schematic

Sampling and Dilution System

The sampling and dilution system was designed to be able to sample flue gas from both, the FR and AR reactors. However, only one reactor, either the AR or the FR, can be sampled at a time. Switching the system from one reactor to the other requires manual manipulation of the sample switching valves. During sampling, the sample is drawn from the flue gas of the reactors with a specially designed sample probe. A schematic of the sample probe is shown in Figure 8.

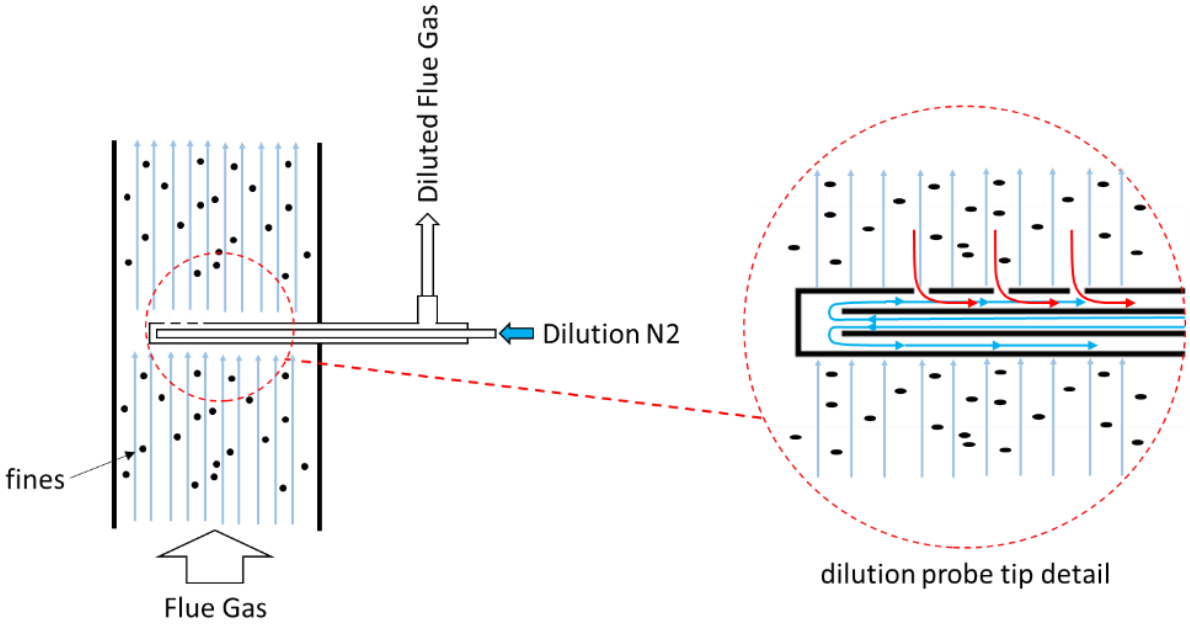

Figure 8 – Alkali sampling probe detail

The probe is designed to simultaneously sample and dilute the flue gas. Dilution nitrogen is delivered to the probe tip via a 3 mm outer diameter tube installed in the center of the 10 mm inner diameter probe body. The sample is sucked from the flue gas through three 1 mm holes. Once the sample enters the probe body it is mixed with the dilution nitrogen and travels out of the probe in the annular space of the probe. The sample probe is mounted to protrude into the center of the flue gas flow and is oriented such that the sample suction direction opposes the flue gas flow direction. This is done in order to minimize ingress of solid fly ash and elutriated oxygen carrier fines.

The diluted sample leaving the sampling probe travels to a porous tube diluter to undergo further dilution by nitrogen. A schematic of the porous tube diluter is shown in Figure 9.

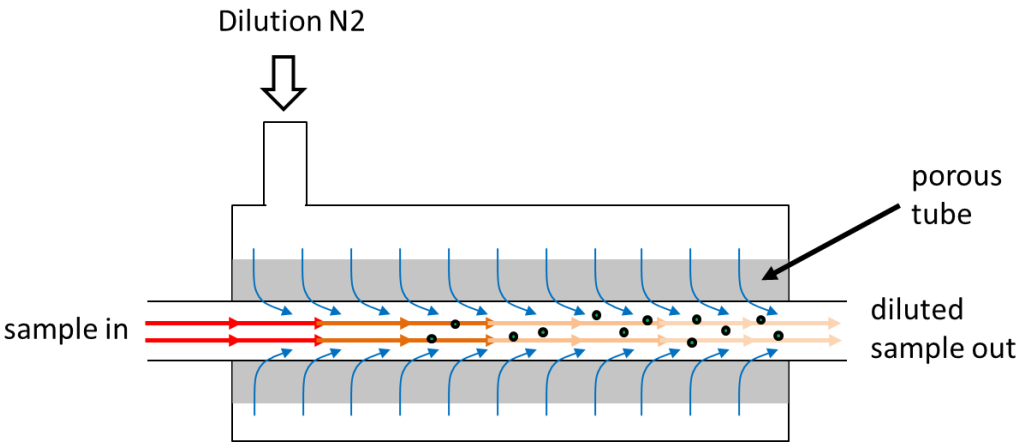

Figure 9 – Porous tube diluter detail

Nitrogen in the porous tube diluter flows inward into the sample path through a porous tube. As the sample travels through the diluter it is diluted and cooled and the residual alkalis present in the sample nucleate to solid particles. From the porous tube diluter, the sample proceeds to the final stage of dilution that is carried out in the Dekati diluter. The Dekati diluter is essentially a venturi device that uses nitrogen as the motive gas and dilution medium. The venturi suction of this diluter is responsible for creating stable sample suction from the process, through the probe and the porous tube diluter. The Dekati diluter expels the diluted sample to the distribution manifold where the flow is split between the SID detector, the CO_2 analyzer (LICOR LI-850), and the trace O_2 analyzer (Alpha Omega Instruments 3000-Y230BTP).

The targeted overall dilution ratio of the system is approximately 50 to 200 times. The dilution ratio has to be adjusted during the sampling campaigns to account for a wide range of alkali emission rates such that the diluted sample alkali concentration is within the calibrated measurement range of the SID detector. In order to control dilution, the nitrogen flows to the sampling probe and the porous tube diluter are controlled by electronic mass flow controllers. Directly setting the dilution rate of the system is not possible since there is no direct measurement of the suction flow, which tends to be unstable due to probe plugging and process pressure variations. Accurate determination of the dilution ratio is critical for recalculating the measured alkali emissions back to raw flue gas basis. When sampling the FR, dilution is tracked using CO_2 as a tracer gas. O_2 is used as the tracer gas when sampling the AR. In both cases, the sampling dilution ratio is calculated by dividing the raw flue gas concentration of the tracer gas (reported by the main process analyzer) by the diluted sample concentration of the tracer gas (reported by the CO_2 and trace O_2 analyzers of the SID measurement system). Details on data processing and calculation of raw flue gas alkali emissions are provided in Chapter 4.

SID Calibration System

Calibration of the SID is carried out by generating a polydisperse aerosol of solid KCl of different mass concentrations and sampling it simultaneously with the SID detector and the

scanning mobility particle sizer (SMPS) (TSI SMPS 3082 & CPC 3750). Comparison of the SID signal against the aerosol's mass concentration, reported by the SMPS, establishes the SID's calibration curve. In the calibration system an aerosol of fine aqueous droplets is generated by an aerosol generator (TSI 3073) using a 0.005 M solution of KCl in deionized water. From the aerosol generator the aqueous aerosol flows through a diffusion dryer. In the dryer the fine aqueous aerosol nucleates into solid KCl particles. The resulting solid KCl aerosol is fed to the SID and the SMPS. The aerosol's mass concentration is controlled by a pressure setting on the aerosol generator. Calibration of the SID system is typically carried out at the start of each measurement campaign day.

CHAPTER 4

4 - Data Processing and Analysis

Data and results relevant to the investigations presented in Papers I through III can be divided into two categories:

1. Data relevant to general CLC system performance
2. Data relevant to alkali investigation

The following sections discuss the data and relevant calculations for both categories.

4.1 CLC Performance Data and Calculations

Although the work presented in this thesis is primarily focused on alkali-specific issues in CLC, this work is invariably tied to efforts to develop biomass CLC technology for efficient carbon capture from thermal conversion of biomass. As such, Papers I and II also evaluate the fuel conversion and carbon capture efficiency of the pilot systems, and perhaps even more importantly, the performance of different combinations of OC materials and biomass fuels. Key performance parameters for CLC operation are discussed below but are all based on the online analysis of FR and AR flue gas composition and process measurements of flow and pressure. Reactor gas analysis was covered in Section 3.3.

Carbon Capture Efficiency

Carbon capture efficiency is arguably the most important parameter in evaluating CLC system performance. There are several ways to calculate carbon capture efficiency of a CLC system, but the most practical method is to calculate the oxide oxygen efficiency. Oxide oxygen efficiency is accepted as a direct equivalent of carbon capture efficiency but is conveniently calculated solely based on measurements of the AR gas composition. Oxide oxygen efficiency is defined as the ratio of the oxygen used for oxidation of the OC in the AR, to the total oxygen consumed in the AR. It is calculated as follows:

$$\eta_{oo}[\%] = 100 * \frac{0.2099 - (1+d)x_{O2,AR} - (1+d)x_{CO2,AR}}{0.2095 - (0.9996+d)x_{O2,AR} - 0.2095x_{CO2,AR}} \quad \text{(Eq.1)}$$

$$\text{Were } d = \frac{\dot{Q}_{dilution\ N2}}{\dot{Q}_{air}} \quad \text{(Eq. 1.1)}$$

In the definition above, d is the ratio of the dilution nitrogen flow introduced into the AR to the AR's fluidizing air flow. The origin of this dilution nitrogen varies for different pilot systems, but typically comes from nitrogen purge gas used for purging pressure taps and from nitrogen used as the fluidization gas in loop seals. Coefficients in Eq. 1 also account for the fact that air fed into the AR contains 400 ppm of CO_2.

Oxygen Demand and Gas Conversion Efficiency

Oxygen demand is another critical parameter in evaluating CLC operation as it reflects the extent of fuel conversion. Oxygen demand is defined as the ratio of the additional oxygen required to fully oxidize the flue gas of the fuel reactor to the stoichiometric oxygen required for complete fuel conversion. Essentially oxygen demand represents an amount of oxygen that is lacking to complete the fuel conversion. Oxygen demand is calculated as follows:

$$\Omega_{OD}[\%] = 100 * \frac{0.5x_{CO,FR} + 2x_{CH_4,FR} + 0.5x_{H_2,FR}}{\Phi_o(x_{CO_2,FR} + x_{CO,FR} + x_{CH_4,FR})} \quad \text{(Eq. 2)}$$

Here Φ_o is the molar ratio [mol O_2 required for combustion/kg fuel] / [mol C/kg fuel].

Gas conversion efficiency is a closely related parameter which indicates the completeness of gas conversion which occurs in the fuel reactor. Gas conversion efficiency is then defined as:

$$\eta_{gas\ conv.}[\%] = 100 - \Omega_{OD} \quad \text{(Eq. 3)}$$

It should be noted, that Ω_{OD} and $\eta_{gas\ conv.}$ parameters do not account for the potential unconverted fuel that escapes with the fuel reactor flue gas as unconverted char. Char loss is typically accounted for separately. Higher order hydrocarbon species (C2, C3, etc.) are also not accounted for, but have been shown from previous CLC operation to be minimal.

Circulation Index

Oxygen carrier circulation is the most important control variable for CLC system operation. Oxygen carrier circulation essentially sets the oxygen carrier residence time in different parts of the CLC system and thus directly affects oxygen transport rates, times available for reaction, in-bed mixing, and other aspects of operation. Circulation cannot be directly controlled but can be manipulated by changing reactor fluidization flows and system inventory. Direct determination of system circulation is very challenging and is very system specific. For this reason, circulation is typically monitored by tracking a proxy variable called the circulation

index (CI). This parameter was used in the study presented in Paper II. CI for the 10 kW CLC pilot is calculated as a product of the AR riser pressure drop and the air flow rate of the AR.

$$CI = \triangle P_{AR\ riser}\ \dot{Q}_{AR\ air} \quad \text{(Eq. 4)}$$

4.2 Alkali Emissions Data and Calculations

Data collected for calculation of alkali emissions measured from the SID consists of the amperage signal measured by the SID, the FR raw flue gas CO_2 concentration measured by the main process gas analyzer, the diluted sample CO_2 and H_2O concentrations measured by the LICOR CO_2 analyzer, the AR raw flue gas O_2 concentration measured by the main process gas analyzer, and the O_2 concentration measured by the Alpha Omega trace O_2 analyzer. Aside from the SID signal, all other data is used solely for the determination of the dilution ratio that is used to correct the alkali concentration measured by the SID. Before calculation of the dilution ratios the diluted CO_2 and O_2 sample concentrations are analyzed to eliminate values which are clearly outside the measurement range of the instruments. Eliminating such values helps improve the integrity of the final calculated alkali concentrations. Dilution ratio for FR alkali measurements are calculated as follows:

$$DR_{FR} = \frac{CO_{2\ FR\ undiluted\ (dry\ basis)}}{CO_{2\ diluted\ sample\ (dry\ basis)}} \quad \text{(Eq. 5)}$$

In Eq. 5, the undiluted CO_2 concentration is reported on dry basis by the main process analyzer. The diluted sample CO_2 concentration, however, is reported on wet basis by the LICOR instrument and must be recalculated to dry basis using the diluted sample H_2O measurement reported by the LICOR analyzer.

For alkali measurements in the AR reactor, O_2 is used as a tracer gas for determining the dilution ratio. Dilution ratio for AR alkali measurements is calculated as follows:

$$DR_{AR} = \frac{O_{2\ AR\ undiluted\ (dry\ basis)}}{O_{2\ diluted\ sample\ (wet\ basis)}} \quad \text{(Eq. 6)}$$

In Eq. 6, the undiluted O_2 concentration is reported on dry basis by the main process gas analyzer. The diluted concentration is reported on wet basis by the Alpha Omega trace O_2 analyzer. Since the AR flue gas contains very little moisture, the diluted sample H_2O content is insignificant. For this reason, the wet basis oxygen concentration of the diluted sample is used in Eq. 6.

Once the dilution ratio of the alkali measurements is calculated, the undiluted raw flue gas concentration is calculated as follows:

$$K_{eq}\left[mg\,\frac{K}{m^3_{normal}}\right] = A_{SID\ 10\,\mathrm{sec}.\,avg.}\ C_{SID}\ DR\ (\frac{298\ K}{273\ K}) \qquad \text{(Eq. 7)}$$

In Eq. 7, K_{eq} is the alkali concentration reported in potassium equivalents in units of mg of potassium per normal m^3, $A_{SID\ 10\,\mathrm{sec}.\,avg.}$ is the SID signal averaged over 10 seconds in units of nanoamperes (nA), C_{SID} is the SID calibration constant in units of mg K/nA, DR is the diltion ratio, and the last factor is temperature correction factor required for calculation on the basis of normal m^3.

The alkali concentration values obtained from the calculation in Eq. 7 are carefully reviewed and outlier values that can result from dilution system instability or from transient events, such as switching the sampling between reactors, are removed to minimize erroneous data. Once the final raw flue gas concentrations are obtained, the mass flowrate of gas-phase alkalis can be calculated as the product of the alkali flue gas concentration and the flue gas flowrate. The flue gas flowrates of both reactors are not measured directly and have to be calculated on the basis of a nitrogen balance. For each reactor, the main gas analyzers report the concentration of CO, CO_2, CH_4, H_2, and O_2. It is assumed that the remainder of the dry gas fraction is composed of N_2.This assumption has been validated in prior operation by directly measuring the N_2 concentration in the reactor flue gases. Thus, the dry basis nitrogen mole fraction can be calculated as:

$$x_{N_2(dry)} = 1 - (x_{CO} + x_{CO_2} + x_{CH_4} + x_{H_2} + x_{O_2}) \qquad \text{(Eq. 8)}$$

The input of N_2 to each reactor is known as it consists of the loop seal fluidization nitrogen, purge nitrogen, and for the AR, the nitrogen that comes in with the fluidizing air. For each reactor system these flows are measured or can be calculated. The fluidization steam input to the FR is also measured on each reactor system. Thus, knowing the flow rate and concentration of N_2 is each reactor and knowing the steam input rate into the FR, reactor flow rates can be calculated as follows:

$$\dot{F}_{AR} = \frac{\sum \dot{F}_{N_{2,AR}}}{x_{N_{2(dry),AR}}} \qquad \text{(Eq. 9)}$$

$$\dot{F}_{FR} = \frac{\sum \dot{F}_{N_{2,FR}}}{x_{N_{2(dry),FAR}}} + \dot{F}_{steam,FR} \qquad \text{(Eq. 10)}$$

The molar flowrates of Eq. 9 and 10, are easily converted to volume basis, using the ideal gas law.

CHAPTER 5

5 - Main Results and Discussion

The results summarized in this chapter cover the experimental work presented in Papers I through III. The results are divided into two main topics

1) Investigation of alkali release in CLC operation
2) Investigation of biomass CLC performance

5.1 Investigation of Alkali Release in CLC of Biomass

Investigating the fate of biomass fuel alkalis in CLC operation was the primary focus of the work presented in Papers I through III. This investigation is divided into several aspects in order to facilitate a systematic discussion of the results.

SID Alkali Measurement System Development

Determining how alkalis are released and distributed in a CLC system was contingent on development of a robust alkali emissions measurement method. The SID principle was chosen as it is relatively simple to implement and has been demonstrated in large-scale operation. However, at the onset of this work it was known that CLC pilot operation is often less stable than industrial scale equipment. CLC pilots often exhibit reactor pressure fluctuations, and typically have significant elutriation of bed material fines to the flue gases of the AR and the FR. For this reason, development of a stable sampling and dilution system was a focal point for the design of the SID alkali measurement system. The basis for the SID system's design was a SID instrument that was used primarily for lab-scale investigations. This design, however, had to be reworked and augmented to make a SID system that is more robust and suitable for CLC operation. The improvement over the base SID design, as developed and implemented in Papers I through III, is captured below:

SID system improvements over base the design, as implemented on the 100 kW CLC pilot (Paper I):

- ***Improved stability of the SID signal:*** Custom designed surface ionization detector instrument with a straight path flow-through design, electronically controlled suction flow rate, and online Pt filament temperature measurement.
- ***Improved sampling stability:*** Custom designed sampling and dilution probe, porous tube diluter, and sample distribution manifold. Dilution nitrogen flows controlled with electronic mass flow controllers.
- ***FR dilution ratio tracking:*** Diluted sample CO_2 tracking for precise determination of FR sample dilution.

SID system improvements over the configuration implemented in Paper I, as implemented on the 10 kW CLC and D-CFB pilots (Papers II and III):

- ***Modularized and portable system:*** The SID alkali measurement system was rebuilt to be modular and transportable, allowing easy transfer between different reactor systems.
- ***AR dilution tracking:*** Implemented diluted sample trace O_2 tracking for precise determination of AR sample dilution ratio.

The SID measurement system that resulted from the development described above is shown in Figure 10. Details are provided in Section 3.4.

Figure 10 – Modular SID alkali measurement system, as setup on the D-CFB pilot

The SID measurement system described above proved to be effective in responding to and measuring alkali emissions during stable operation and during transient operational events

such as fuel feed startup and shutdown. This was first demonstrated in Paper I, and later confirmed in Papers II and III. However, fast transient events, such as switching the sampling between the AR and the FR proved to cause temporary signal instability. To avoid this reading instability, signal data corresponding to abrupt transient events of sample switching or sample probe flushing was removed at the data processing stage.

Alkali Release Results

Alkali emissions measurements were collected in the three studies presented in Papers I through III. The main observations of the measurements are summarized in the following sub-sections.

Alkali Emissions vs. Fuel Alkali Content

The results from all three experimental studies clearly show that the alkali release in the FR rises with the alkali content of the biomass fuel. Figure 11 summarizes the average FR alkali emissions. Results from Papers I through III are presented with the emissions figures recalculated to a basis of mg K_{eq}/kg fuel, in order to make the results comparable. Fuels are listed in order of increasing alkali content. Each fuel's alkali content, in units of mg alkali per kg fuel, is included in parentheses. FR emissions for Paper III tests with braunite OC are plotted on a secondary axis for easier visual comparison to other test results.

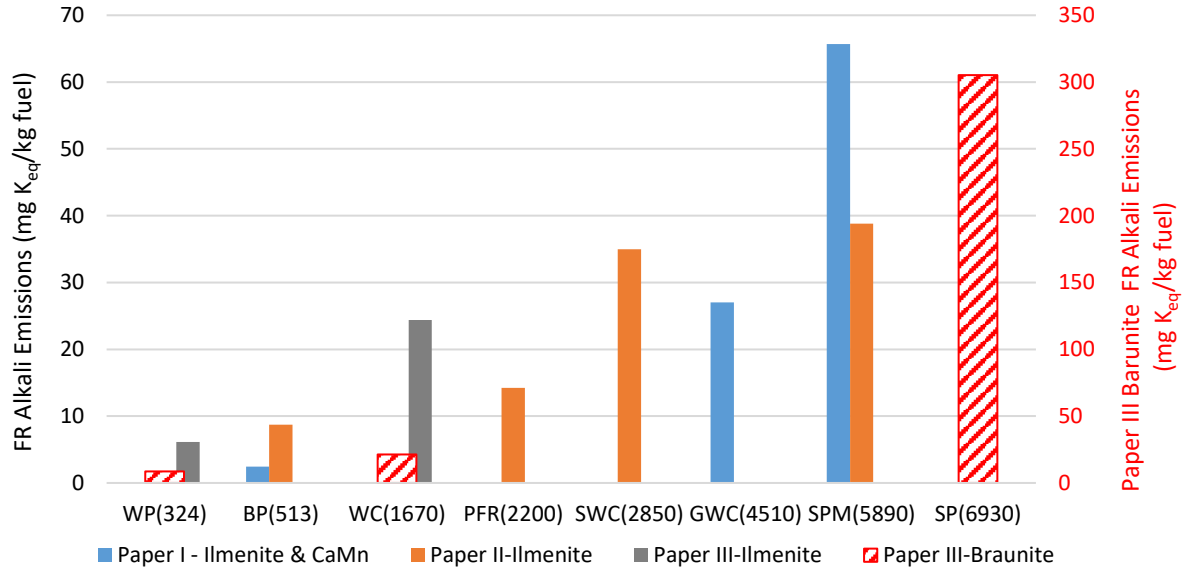

Figure 11 - Average FR alkali emissions (Papers I – III)

Figure 11 clearly shows that fuel alkali emissions grow with increasing fuel alkali content. This observation is consistent for all studies. One fuel, black pellets doped with K_2CO_3, is excluded from the results as it is not representative of biomass fuel. In Paper I, it was found that despite having an alkali content of 12000 mg K/kg fuel, this fuel results in alkali emissions that are only slightly higher than that of undoped black pellets. The ineffective gas-phase release of K from

the added K_2CO_3 was attributed to its loose and coarse powder form. This form is not representative of how fuel alkalis are present in biomass and thus might behave completely differently from alkalis of biomass origin.

AR alkali emissions for CLC operation in experiments presented in Papers I through III are presented in Figure 12. AR emissions for Paper III tests with braunite OC are plotted on a secondary axis. In this figure, AR emissions for ilmenite tests in Papers II and III show no dependency of AR alkali release on the fuel's alkali content. Results for Paper I show a significant increase in AR alkali emissions as fuel is changed from black pellets (BP) to straw pellet mix (SPM). It should be noted, however, that the AR results presented for Paper I are approximate. In Paper I, the SID alkali measurement system was at the early stage of development and tracking of AR sample dilution was not yet implemented. Results for the braunite tests in Paper III show that AR emissions grow with increasing fuel alkali content.

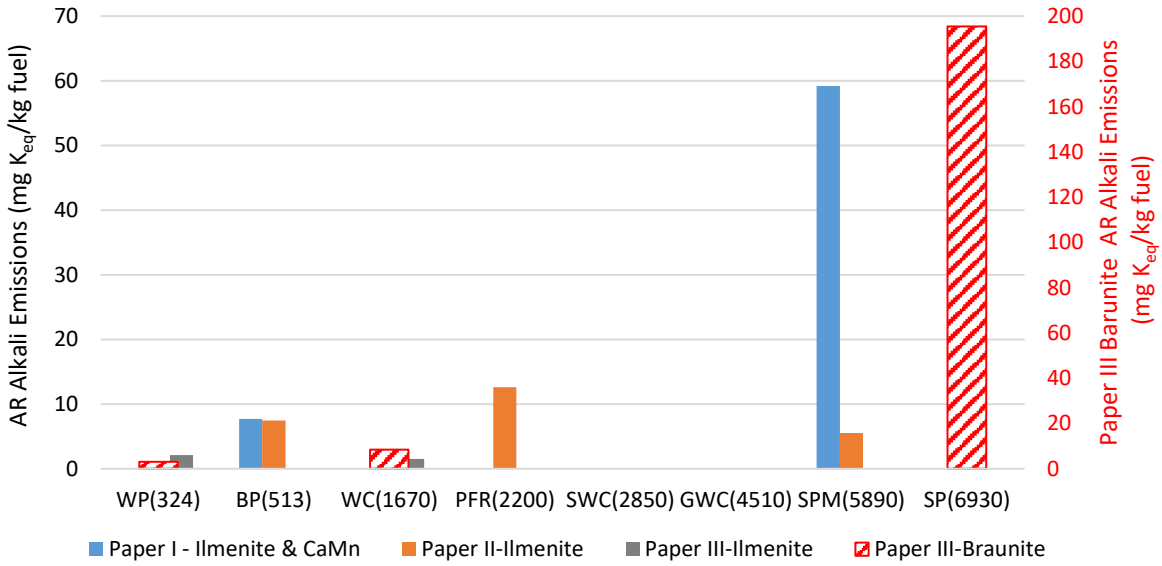

Figure 12 - Average AR alkali emissions (Papers I – III)

Due to the difference in results from the different studies, the effect of fuel alkali content on AR alkali emissions is difficult to ascertain. It is quite possible that the process for AR alkali release has a higher dependency on factors other than the fuel itself. Further discussion on the origin of AR alkali emissions is continued in the next subsection.

Distribution of Alkalis in a CLC system

Distribution of alkali release in the CLC system was explored in Papers I through III. The measured alkali emissions from the AR and the FR were compared to the alkali input by the fuel. Table 7 provides a summary of average relative alkali distributions from Papers I - III.

Table 7 – Relative alkali distribution in CLC operation (Papers I – III)

		Paper I Ilmenite & CaMn		Paper II Ilmenite		Paper III Ilmenite		Paper III Braunite	
Fuel	**mg alkali/kg fuel**	**FR**	**AR**	**FR**	**AR**	**FR**	**AR**	**FR**	**AR**
WP	324					1.9%	0.7%	2.9%	1.0%
BP	513	0.7%	1.8%	1.7%	1.5%				
WC	1670					1.3%	0.1%	1.3%	0.5%
PFR	2200			0.7%	0.6%				
SWC	2850			1.2%					
GWC	4510								
SPM	5890	1.1%	1.1%	0.7%	0.1%				
SP	6930							4.4%	2.8%

Table 7 shows that overall release of alkalis to the gas phase of both reactors is in the range of 0.8% to 7.2%. Surprisingly, the release occurs at significant levels in both the FR and the AR. AR emissions appear to be in the same range as the FR emissions for most tests in Papers I and II. AR emissions are distinctly lower in operation with the straw pellet mix (SPM) in Paper II. In Paper III, AR emissions are about 40% to 70% lower in the AR than in the FR. In all cases, the AR emissions are significant. This result is somewhat unexpected, as at the onset of this work it was hypothesized that the vast majority of alkali emissions will occur in the FR. This hypothesis was based on the fact that biomass fuel is known to be converted in the FR.

Since no fuel is fed into the AR during CLC operation, the alkalis released in the AR must be transported from the FR. One possibility is that some fraction of the solid biomass fuel is not fully converted in the FR and some unconverted char is carried over to the AR along with the circulating bed material. Studies measuring release of alkalis from biomass report that only <10% of alkalis are typically released in the devolatilization stage of fuel decomposition [38,40]. Thus, the char left after devolatilization can contain >90% of the fuel's alkalis. After devolatilization, the temperature of the remaining char continues to rise towards the FR bed temperature, while steam gasification begins. As the temperature rises, the primary gas-phase release of alkalis comes from evaporation of KCl, followed by decomposition of alkali carbonates and sulphates. Knudsen et al. [38] measured and modelled the high temperature dissociation reaction rates for potassium carbonates, sulphates, and silicates. Their work showed that carbonates begin to dissociate above 700^{o}C, sulphates above 900^{o}C, and silicates above 1200^{o}C. At the temperature of the FR, approximately 900-970^{o}C, the dissociation rate of KCl is fast, so release of KCl to the gas phase likely proceeds to completion. The dissociation rate of K_2CO_3 is slower, and very slow for K_2SO_4. Thus, with limited residence time in the FR, the unconverted char may carry over undissociated potassium carbonates and sulphates over to the AR. Another possibility for carryover is that alkalis that are trapped in a condensed phase during fuel ash formation are also carried over to the AR by the bulk transport along with the oxygen carrier. Ash can contain alkalis as silicates, but also possibly as undecomposed carbonates and sulphates.

With either mode of transport, char-bound or ash-bound, condensed alkalis can continue their release to the gas phase in the AR. The bed temperature of the AR is typically 50°C to 100°C higher than that of the FR. Thus, the carried over ash is exposed to higher temperature in the AR than in the FR. This is also true for carried over char, although char readily combusts in the AR and likely reaches local temperatures higher than that of the AR bed. In either case, the higher temperature accelerates dissociation of the carried over alkali compounds. The dissociation rate models from Knudsen et al. [38], show that for every 100°C of temperature rise, potassium carbonate and sulphate dissociation rates increase roughly by a factor of 10. Thus, in the hotter environment of the AR the carried over alkali carbonates and sulphates likely continue to release to the gas phase, and do so at higher rates. For the char-bound transport case, it may even be possible that the local combustion temperatures of the carried over char particles can cause dissociation of alkali silicates, which is known to occur above 1200°C [38].

Estimating char slippage to the AR can be done by considering the carbon capture efficiency of the CLC system. Average carbon capture performance for the tests in Papers I and II is presented in Table 8. The carbon capture efficiency for experiments in Paper III is currently being evaluated, so only preliminary estimates of carbon capture efficiency are shown for experiments in Paper III.

Table 8 – Average carbon capture efficiency (Papers I – III)

Fuel	Paper I Ilmenite & CaMn	Paper II Ilmenite	Paper III Ilmenite	Paper III Braunite
WP			<90%	<90%
BP	99.4%	99.0%		
WC			<60%	<60%
PFR		98.2%		
SWC		95.4%		
SPM	98.1%	97.3%		
SP				<80%

From Table 8, carbon capture efficiency for experiments in Papers I and II range from 95% to 99%. For these experiments, the average slippage of unconverted char over to the AR can be estimated to be at approximately 1% to 5% to of the fuel's total carbon content. For experiments in Paper III, the carbon capture efficiency is quite poor and char slippage to the AR can range from 10% to 40% of the fuel's total carbon content. Thus, especially for experiments in Paper III, char slippage to the AR is probably responsible for a significant portion of the alkalis that are released to the gas phase in the AR.

The above-described char and ash alkali carryover and release mechanisms constitute the best hypothesis for explaining the observed AR emissions. These mechanisms need further experimental validation and may not fully explain the magnitude of the AR alkali emissions.

Alkali Retention

Retention of alkalis in the reactor, either retained in the bed material or in the elutriated solids, can be estimated as the difference between the incoming fuel alkalis and the alkalis detected in the FR and AR flue gases. Table 9 presents calculated alkali retention for experiments presented in Papers I through III.

Table 9 – Alkali retention in the reactor system (Papers I – III)

Fuel	mg alkali/kg fuel	Paper I Ilmenite & CaMn	Paper II Ilmenite	Paper III Ilmenite	Paper III Braunite
WP	324			97.5%	96.9%
BP	513	97.5%	96.8%		
PFR	2200		98.7%		
WC	1670			98.6%	98.2%
SWC	2850				
SPM	5890	97.8%	99.2%		
SP	6930				92.8%

From Table 9 it is apparent that alkali retention is high for all fuels and similar for all oxygen carriers. Although these figures were calculated solely based on alkali emissions measured by the SID, these high retention rates have also been confirmed by analysis of alkali accumulation in the bed material and the solid material captured by the flue gas filters in Papers I and II. It is well-known that even without the presence of oxygen carrier, some alkali species are retained in a condensed phase through the process of ash formation. Controlled experiments investigating gas phase alkali release at grate firing conditions report that approximately 20-40% of fuel alkalis are released for woody and annual biomass [41,52]. The remaining 60-80% of the fuel alkalis are retained in ash that is left after fuel conversion. Since grate firing conditions imply no extraneous matter, retention of 60-80% of the fuel's alkalis can be attributed to ash formed in fuel decomposition, without accounting for the influence of the oxygen carrier. The remaining approximately 10-30% of alkali retention can be attributed to the effects of the oxygen carriers. Exactly how the oxygen carriers influence the retention is difficult to ascertain in pilot-scale experimental investigations. However, several interactions of the oxygen carrier materials with alkalis are known. Firstly, the major components of both ilmenite and braunite can react with alkali species. For ilmenite, it is well known that K can be captured by the TiO_2 fraction by forming stable potassium titanates [44,53,54]. For braunite, which is a manganese ore, formation of potassium manganates has been demonstrated in ash interaction experiments with Mn/Si-based OC materials and K_2CO_3 salts [55]. Beyond the major components of these oxygen carriers, Si and Al are present in significant amounts in both oxygen carriers. These species are known to readily react with alkalis to form alkali silicates or aluminosilicates.

Effect of Reactor Atmosphere on Gas-phase Alkali Release

The effect of reactor atmosphere was investigated in Paper III. Tests on the D-CFB reactor system were performed in two distinct combustion modes: oxygen carrier aided combustion (OCAC), and CLC. OCAC is essentially conventional fluidized bed combustion, but with an oxygen carrier used as a bed material instead of sand [56]. In OCAC, the oxygen carrier helps in buffering oxygen distribution in the bed, and when operated with ilmenite, helps mitigate alkali related issues though ilmenite's ability to absorb alkali. In terms of fuel conversion, OCAC is most like a conventional fluidized bed combustion process, where most of the fuel is oxidized with air. In Paper III, fueled experiments stared with OCAC conditions, and were followed by a switch to CLC operation. Alkali emissions measurements for both tested oxygen carriers, and most fuels, showed that a switch from OCAC to CLC was accompanied with a distinct rise in FR alkali emissions. Figure 13 shows an example of such a transition for a test with ilmenite and wood char (WC) fuel.

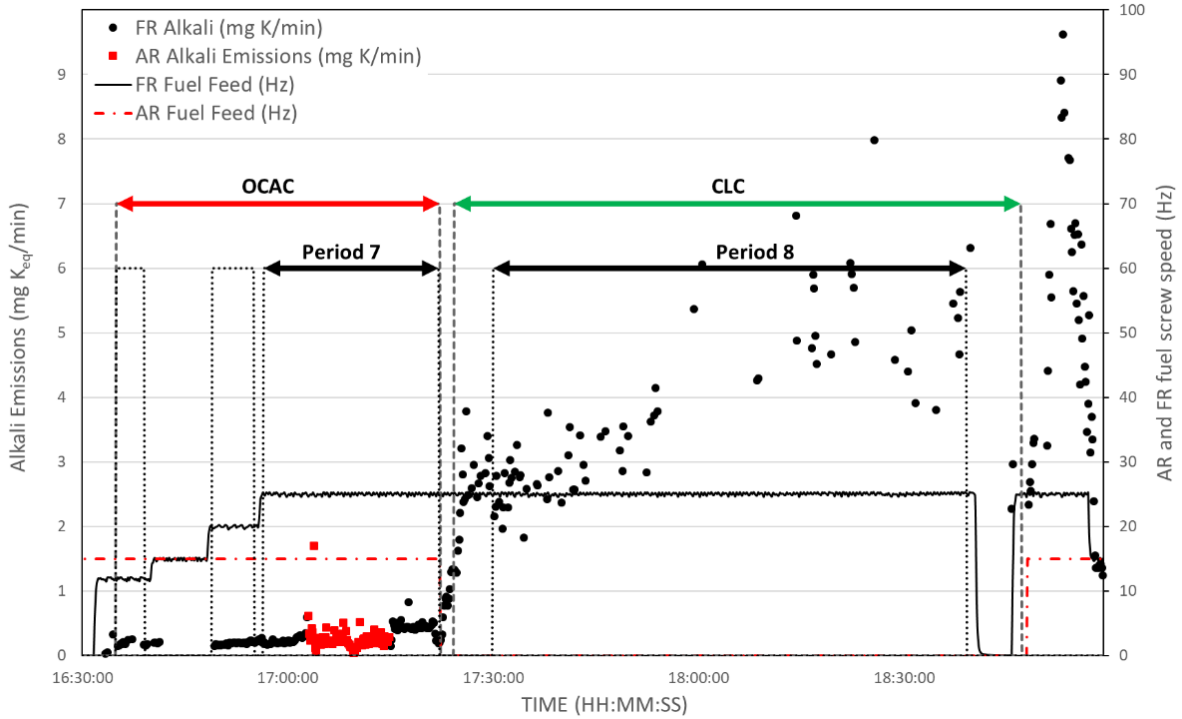

Figure 13 – Alkali emissions for ilmenite & wood char (Paper III)

In Figure 13, despite a constant fuel feed to the FR, alkali emissions increase drastically in response to switching the FR atmosphere from air fluidization to fluidization with steam (to start CLC operation). This effect is consistent for almost all fuels, but is most noticeable for fuels of higher alkali content. FR alkali emissions for combustion and CLC operation are summarized in Table 10.

Table 10 – Average FR alkali emissions for OCAC and CLC tests (Paper III)

OC Material	Fuel	mg alkali/kg fuel	OCAC FR emissions (mg K/kg fuel)	CLC FR emissions (mg K/kg fuel)	% increase with CLC
Ilmenite	**WP**	324	1.9	6.1	217%
	WC	1670	2.3	24.4	983%
Braunite	**WP**	324	9.2	8.7	-5%
	WC	1670	3.2	21.4	564%
	SP	6930	19.4	305.3	1470%

To help the comparison of OCAC and CLC FR emissions, the results presented in Table 10 have been recalculated from the original data presented in Paper III to a basis of 1 kg of fuel input. Except for tests with braunite and wood pellets, Table 10 shows that CLC operation results in a clear and significant increase in FR alkali emissions. The reason for this effect is explored in the results and discussion section of Paper III. The analysis presented in Paper III examines the fuel decomposition process and relies on results of alkali release experiments and theory from literature. Fuel alkali release paths are considered in the context of the staged fuel decomposition processes that occurs in OCAC and CLC conditions. The analysis concludes that the alkali release is likely similar in the common process of gas-phase alkali release in devolatilization, and gas-phase alkali release through high temperature evaporation of KCl. The apparent difference in gas-phase alkali release is attributed to the different conditions for char conversion in OCAC and CLC operation. As evidenced by several studies [57,58], steam is known to accelerate the decomposition of K_2CO_3 and K_2SO_4 through formation of KOH(g).The increased emissions in CLC are attributed to the alkali release that comes from accelerated decomposition of alkalis that are present in the fuel char in carbonate and sulfate forms.

It is important to emphasize that the gas-phase alkali release in CLC experiments in Paper III is high in comparison to OCAC, but not necessarily in comparison to conventional circulating fluidized bed (CFB) combustion. The difference between OCAC and CFB combustion is that OCAC uses an oxygen carrier as the bed material, while CFB operations typically use sand. As shown in Paper III, oxygen carriers themselves can affect alkali release and retention. This ability is likely quite different from the sand's known tendency to form sticky silicate melts with biomass alkalis.

Effect of CLC Reactor Control Parameters on Alkali Release

Along with investigating alkali release, Papers I and II of this thesis evaluate the overall system performance of two CLC pilots, the 100 kW pilot and the 10 kW pilot. Conclusions on general system performance are included in Section 5.2, but the interaction of CLC control parameters with alkali release are briefly discussed here. Generally, for a fixed reactor-OC-fuel combination, the main CLC system control parameters are the operating temperature and solids circulation. Unfortunately, the effect of operating temperature was not explored in Studies I through III but is being explored in an upcoming experimental campaign. The effect of solids circulation, however, was explored in Studies I and II. For the 10 kW and 100 kW CLC

pilots, solids circulation is primarily controlled by the air flowrate in the AR and the system's OC inventory. In Studies I and II, the alkali concentration was compared to changes in AR flowrate, changes to system inventory, and to the calculated circulation index. No apparent effect of these parameters on the release of alkalis was found. This finding is important as it suggests that the alkali release likely does not significantly constrain these control variables. Since OC circulation has a direct effect on gas conversion efficiency of volatile fuels, as will be shown in Section 5.2, the independence of alkali emissions from solid circulation rates is beneficial for operating flexibility.

5.2 Investigation of biomass CLC process performance

In parallel to determining the behavior of alkali release in CLC, the work in this thesis also addressed overall development of the biomass CLC technology. From the experimental perspective, the most important aspects of improving biomass CLC technology are reactor development and oxygen carrier selection.

Commissioning and Performance Evaluation of a New 10 kW CLC Pilot (Paper II)

A major biomass CLC reactor development effort is captured in the work presented in Paper II of this thesis. In this study, a new 10 kW solid fuels reactor, designed specifically for use of high volatiles biomass, was commissioned. The design of this reactor is described briefly in Section 3.1 of this thesis, and in detail in Paper II. The new reactor design was based on a first-generation solid fuels CLC pilot but includes multiple improvements. The key improvements are:

- Implementation of a larger and taller FR geometry to increase OC and fuel residence time
- Implementation of a volatiles distributor to help increase contact between biomass volatiles and the OC material
- Removal of the carbon stripper (implemented in the 1st generation reactor) in order to decrease system complexity

Commissioning of this new reactor spanned six operational days, with over 21 hours of fueled CLC operation. Ilmenite was used as the oxygen carrier and 4 different biomass fuels of varying volatiles and alkali content were tested. Table 11 presents a summary of the system's performance benchmark tests.

Table 11 – 10 kW CLC pilot performance summary (Paper II)

Fuel	Reactor OC Inventory (kg)	FR Temp. (°C)	P_{fuel} (kW)	η_{oo} (%)	$\eta_{gas\ conv.}$ (%)
BP	39.4	982	7.1	99.2	78.5
SWC	25.0	986	5.7	94.8	94.5
PFR	38.3	960	6.0	98.6	75.7
SPM	35.4	909	7.2	96.1	74.9

The key performance metrics shown in Table 11 are the oxide oxygen efficiency (η_{oo}), which is equivalent to carbon capture efficiency, and the gas conversion efficiency ($\eta_{gas\ conv.}$). The carbon capture efficiency achieved in the new unit was quite high, >94% for low volatiles biomass and >96% for high volatiles biomass. These numbers are close to the carbon efficiencies reported on the previous generation unit, see Table 8 in Paper II, but are achieved without the need of a carbon stripper. This can be considered a significant design improvement, since the new reactor design is simplified without compromising carbon capture efficiency. The gas conversion efficiency reported is also quite high, when compared to gas conversion efficiencies achieved in the 1st generation 10 kW unit and the 100 kW unit. A detailed discussion and comparison of gas conversion efficiencies are included in Paper II, see Table 10 and discussion in Paper II. From this comparison, it is concluded that the new 10 kW CLC pilot can achieve gas conversion improvement of up to 10 percentage points for high-volatiles biomass fuels. This significant improvement is concluded to be the result of improved contact between the fuel's volatiles and the OC material that is facilitated by the volatiles distributor.

Further performance evaluation of the new 10 kW CLC reactor establishes that, aside from operating temperature and the choice of oxygen carrier, the system's solids circulation rate is the most important variable influencing system performance. The effect of solids circulation in the 10 kW CLC reactor system is shown in Figure 14, as replicated from Paper II.

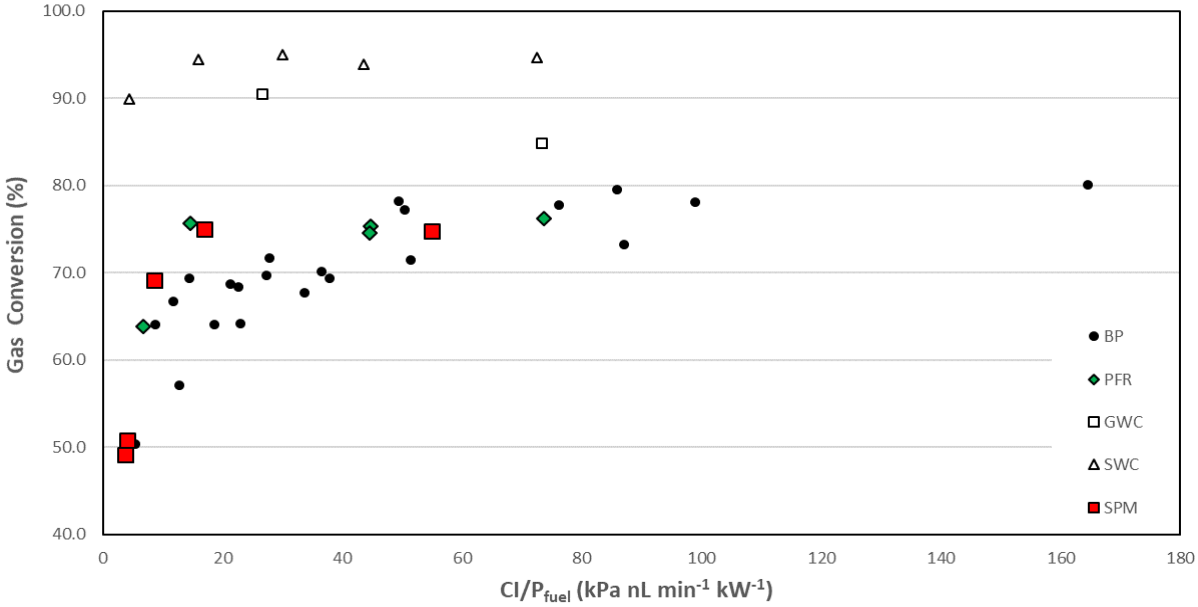

Figure 14 – Gas conversion efficiency vs. power-specific circulation index (Paper II)

Figure 14 shows that increased system circulation, represented here as power-specific circulation index (CI/P_{fuel}), improves gas conversion efficiency for high-volatiles biomass fuels. This effect is attributed to the fact that higher OC circulation results in lower OC reduction in the FR, and thus higher OC reactivity. The low-volatiles char fuels, GWC and SWC, are not affected by be OC circulation rate since their volatiles release is low, thus having a higher OC to volatiles ratio. The higher OC to volatiles ratio allows the conversion reactions to achieve a higher degree of completion even at lower oxygen carrier reactivities.

Performance of Ilmenite and Calcium Manganite Mixed OC (Paper I)

Performance investigation of a mixed OC material consisting of ilmenite and synthetic calcium manganite material was carried out in Paper I in a 100 kW CLC pilot unit. Evaluation of the system's performance concluded that carbon capture efficiencies between 97% to 100% are achievable. It was also shown that the calcium manganite additive effectively boosts gas conversion efficiency. Gas conversion efficiencies of 95-97% were achieved with black pellets fuel. This is a great improvement over the maximum gas conversion efficiencies of 75% achieved in the same reactor with black pellets fuel and manganese ore OC material [20]. The gain in gas conversion efficiency was attributed to the oxygen uncoupling effect of the calcium manganite material. More detailed discussion and results are presented in Paper I.

CHAPTER 6

6 - Summary and Conclusions

Chemical looping combustion of biomass is a promising technology that enables thermal conversion of biomass fuels with inherent carbon dioxide capture. Since biomass itself is carbon neutral, CLC of biomass is a negative emissions technology whose development may be critical for combatting climate change. The experimental work presented in this thesis was focused on resolving challenges to the development and implementation of biomass CLC. The primary focus was on investigating alkali-related issues in CLC. Specifically, the studies focused on determining how biomass alkalis are released in the CLC process. The alkali investigation was complemented with experimental evaluation of a new oxygen carrier material and commissioning and evaluation of a new CLC pilot reactor. In total, three experimental studies were conducted using three different CLC pilot systems, three different oxygen carriers, and 9 different biomass fuels. A total of 50 hours of operation was conducted at CLC conditions.

A major effort for enabling investigation of alkali release in pilot scale experiments was the development of a robust online alkali measurement system. This effort led to designing and constructing a surface ionization detector (SID), a sampling and dilution system, and a calibration system. Together these systems were built into a complete modular and transportable online alkali measurement system. The resulting alkali measurement system was successfully implemented in prototype form in experiments detailed in Paper I, and in completed form in experiments presented in Papers II and III. Measurement performance of the system was proven to be stable, as evidenced by the agreement of the alkali release measurements collected in the three studies. The sensitivity of the system was also deemed sufficient, with the measurement system able to respond to operational changes.

Alkali measurements for both the FR and the AR were conducted in all three experimental studies. Analysis of the measurements showed that approximately 1-10% of fuel alkalis are released to the gas phase during chemical looping combustion operation. The overall gas phase release was found to correlate with the fuel's alkali content, with high alkali fuels releasing more alkalis to the gas phase. Looking at each reactor separately showed that it is

primarily the FR emissions that consistently correlate with the fuel's alkali content. The AR alkali emissions correlated with the fuel's alkali content in several cases, but a definitive trend was not established. Comparing the relative distribution of the gas-phase alkali release, revealed that significant release occurs in both, the FR and the AR. In several cases, AR alkali emissions were reported to be even higher than those of the FR. This was more typical for fuels with low alkali content. CLC operation with high alkali biomass fuels resulted in the FR exhibiting higher gas phase alkali emissions in most cases.

The few cases where AR alkali emissions were equal or higher than those of the FR, constitute an important finding. The presence of significant alkali emissions in the AR directly opposes this work's original main hypothesis that most of the alkali emissions are expected to occur in the FR. Investigation of the process conditions and review of alkali release theory led this work to a preliminary conclusion that alkali emissions in the AR most likely occur due to char carryover from the FR, whereby the char burns in the AR releasing char-bound alkalis. Another possibility is that some alkalis are transported to the AR as fuel ash in carbonate and sulphate forms, which release to the gas phase in the AR due to the AR's higher temperature. It should be noted that these conclusions are preliminary and will be investigated in further pilot and lab-scale studies.

Another key finding with respect to gas-phase alkali release was discovered in comparing OCAC and CLC operation in experiments presented in Paper III. It was found that CLC operation exhibits higher gas-phase alkali emissions when compared to emissions from OCAC tests performed using the same reactor, oxygen carrier, and fuel. Analysis of this behavior concluded that the higher emissions in CLC operation likely occur due the steam atmosphere in CLC operation. Is was concluded that, most likely, steam increases the release of alkalis from carbonate and sulphate alkali species that are present in the fuel char during the gasification step of CLC.

Beyond observations of gas-phase alkali release, all three studies established that more than 97% of all fuel alkalis are retained in condensed form. This was confirmed by elemental analysis of the bed material samples in Studies I and II. Review of the possible mechanisms of alkali retention led to a conclusion that up to 80% of the alkali retention can be attributed to ash formation processes that occurs during fuel decomposition. The residual retention occurs due oxygen carrier interaction with the fuel's inorganic content. For the two ilmenite-containing oxygen carriers it was concluded that alkalis are probably primarily trapped through formation of alkali silicates, aluminosilicates, manganates and titanates. For the braunite OC it was concluded that alkalis are probably primarily trapped through formation of alkali silicates, aluminosilicates and manganates.

Alongside the alkali investigation, this work also contributed to the progress of biomass CLC technology. Experiments presented in Paper I evaluated the performance of an ilmenite and calcium manganite mixed OC material. There, it was found that addition of synthetic calcium manganite material to ilmenite oxygen carrier helps reach overall gas conversion efficiency of

up to 97% for biomass fuels, a remarkable increase compared to around 75% with manganese ore. Experiments presented in Paper II commissioned a newly designed CLC pilot reactor that was tailored for operation with high volatiles biomass. Evaluation of this pilot reactor showed that the new design can achieve carbon capture efficiency >96% and gas conversion efficiency of up to 80%, when operated with high volatiles biomass fuel. This gas conversion figure represents an improvement of up to 10 percentage points vs. the previous generation design and was concluded to be a result of implementing a novel volatiles distributor concept in the FR internals. The investigation of reactor performance also established that higher OC material circulation significantly improves gas conversion efficiency for high volatiles biomass fuels. Both CLC performance investigations presented in Papers I and II also looked at the interdependencies of typical CLC system control parameters with gas-phase alkali emissions. No significant interdependencies were found in the conducted experiments. It was concluded that CLC system control parameters are likely not constrained by alkali release behavior.

Nomenclature

AR	*air reactor*
BECCS	*bioenergy with carbon capture and storage*
BP	*black pellets*
CFB	*circulating fluidized bed*
CLC	*chemical looping combustion*
CLOU	*chemical looping with oxygen uncoupling*
CPC	*condensation particle counter*
CR	*circulation riser*
CS	*carbon stripper*
D-CFB	*dual circulating fluidized bed*
ELIF	*laser induced fragmentation fluorescence*
FR	*fuel reactor*
GWC	*German wood char*
ICP-OES	*inductively-coupled plasma optical emission spectroscopy*
IPCC	*intergovernmental panel on climate change*
LLS	*lower loop seal*
LS	*loop seal*
MFC	*mass flow controller*
NETs	*negative emissions technologies*
OC	*oxygen carrier*
OCAC	*oxygen carrier aided combustion*
PFR	*pine forest residue*
SMPS	*scanning mobility particle sizer*
SPM	*straw pellet mixture*
SP	*straw pellets*
SID	*surface ionization detector*
SWC	*Swedish wood char*
TDLAS	*tunable diode laser absorption spectroscopy*
ULS	*upper loop seal*
VDC	*volts, direct current*
VTDMA	*volatility tandem mobility analysis*
WC	*wood char*
WP	*wood pellets*

$\boldsymbol{m_{oc,i}}$	*mass of oxygen carrier in section i, in kg*
$\boldsymbol{\delta}$	*perovskite oxygen deficiency factor*
$\Delta\boldsymbol{P_i}$	*pressure drop over section i, in Pa*
$\boldsymbol{\dot{F}_{i,j}}$	*flow of gas i in section j, in mol/min*
$\boldsymbol{CI}$	*dimensionless circulation index*
$\boldsymbol{\dot{Q}_{i,j}}$	*flow of gas i in section j, in m^3_{normal}/min*
$\boldsymbol{\eta_{oo}}$	*oxide oxygen efficiency, in %*
$\boldsymbol{x_{i,j}}$	*mole fraction of gas i in reactor j*
$\boldsymbol{d}$	*dimensionless nitrogen dilution ratio*
$\boldsymbol{\Omega_{OD}}$	*oxygen demand, in %*
$\boldsymbol{\eta_{gas\ conv.}}$	*gas conversion efficiency, in %*
$\boldsymbol{DR_j}$	*dimensionless dilution ratio in reactor j*
$\boldsymbol{\Phi_o}$	*ratio of moles of O_2/kg of fuel to moles of C/kg of fuel*

References

[1] Yongsung C, Davis SJ, Jackson RB, Lowe J, Rogner M, Kraxner F, et al. Biophysical and economic limits to negative CO2 emissions. Nat Clim Chang 2015;6:42–50. doi:10.1038/nclimate2870.

[2] Pachauri RK, Meyer L, Hallegatte France S, Bank W, Hegerl G, Brinkman S, et al. Climate Change 2014: Synthesis Report. Contribution of Working Groups I, II and III to the Fifth Assessment Report of the Intergovernmental Panel on Climate Change. Gian-Kasper Plattner; 2014.

[3] Lyngfelt A, Leckner B, Mattisson T. A fluidized-bed combustion process with inherent CO2 separation; Application of chemical-looping combustion. Chem Eng Sci 2001;56:3101–13. doi:10.1016/S0009-2509(01)00007-0.

[4] Kobayashi, N.; Fan L-S. Biomass direct chemical looping process: A perspective. Biomass and Bioenergy 2011:1252–62.

[5] Noorman S, van Sint Annaland M, Kuipers JAM. Experimental validation of packed bed chemical-looping combustion. Chem Eng Sci 2010;65:92–7. doi:10.1016/j.ces.2009.02.004.

[6] Iloeje CO, Zhao Z, Ghoniem AF. Design and techno-economic optimization of a rotary chemical looping combustion power plant with CO2 capture. Appl Energy 2018;231:1179–90. doi:10.1016/j.apenergy.2018.09.058.

[7] Mukherjee S, Kumar P, Yang A, Fennell P. Energy and exergy analysis of chemical looping combustion technology and comparison with pre-combustion and oxy-fuel combustion technologies for CO<inf>2</inf> capture. J Environ Chem Eng 2015;3:2104–14. doi:10.1016/j.jece.2015.07.018.

[8] Lyngfelt A, Leckner B. A 1000 MW th boiler for chemical-looping combustion of solid fuels – Discussion of design and costs. Appl Energy 2015;157:475–87. doi:10.1016/j.apenergy.2015.04.057.

[9] Zhu L, He Y, Li L, Wu P. Tech-economic assessment of second-generation CCS: Chemical looping combustion. Energy 2018;144:915–27. doi:10.1016/j.energy.2017.12.047.

[10] Keller M, Kaibe K, Hatano H, Otomo J. Techno-economic evaluation of BECCS via chemical looping combustion of Japanese woody biomass. Int J Greenh Gas Control 2019;83:69–82. doi:10.1016/j.ijggc.2019.01.019.

[11] Lyngfelt A, Brink A, Langørgen Ø, Mattisson T, Rydén M, Linderholm C. 11,000 h of chemical-looping combustion operation—Where are we and where do we want to go? Int J Greenh Gas Control 2019;88:38–56. doi:10.1016/j.ijggc.2019.05.023.

[12] Lyngfelt A, Linderholm C. Chemical-Looping Combustion of Solid Fuels - Status and

Recent Progress. Energy Procedia 2017;114:371–86. doi:10.1016/j.egypro.2017.03.1179.

[13] Basu P. Biomass gasification, pyrolysis and torrefaction: Practical design and theory. 2018. doi:10.1016/C2016-0-04056-1.

[14] Gu H, Shen L, Xiao J, Zhang S, Song T. Chemical looping combustion of biomass/coal with natural iron ore as oxygen carrier in a continuous reactor. Energy and Fuels 2011;25:446–55. doi:10.1021/ef101318b.

[15] Gu H, Shen L, Zhong Z, Zhou Y, Liu W, Niu X, et al. Interaction between biomass ash and iron ore oxygen carrier during chemical looping combustion. Chem Eng J 2015;277:70–8. doi:10.1016/j.cej.2015.04.105.

[16] Adánez-Rubio I, Abad A, Gayán P, De Diego LF, García-Labiano F, Adánez J. Biomass combustion with CO2capture by chemical looping with oxygen uncoupling (CLOU). Fuel Process Technol 2014;124:104–14. doi:10.1016/j.fuproc.2014.02.019.

[17] Mendiara T, Abad A, de Diego LF, García-Labiano F, Gayán P, Adánez J. Biomass combustion in a CLC system using an iron ore as an oxygen carrier. Int J Greenh Gas Control 2013;19:322–30. doi:10.1016/j.ijggc.2013.09.012.

[18] Pikkarainen T, Hiltunen I. Chemical looping combustion of solid biomass–performance of ilmenite and braunite as oxygen carrier materials. 2017.

[19] Langørgen Ø, Saanum I. Chemical Looping Combustion of wood pellets in a 150 kW th CLC reactor. Proc. Int. Conf. Negat. CO2 Emiss., 2018, p. 1–10.

[20] Schmitz M, Linderholm C. Chemical looping combustion of biomass in 10- and 100-kW pilots – Analysis of conversion and lifetime using a sintered manganese ore. Fuel 2018;231:73–84. doi:10.1016/j.fuel.2018.05.071.

[21] Cho P, Mattisson T, Lyngfelt A. Comparison of iron-, nickel-, copper- and manganese-based oxygen carriers for chemical-looping combustion. Fuel 2004;83:1215–25. doi:10.1016/j.fuel.2003.11.013.

[22] Leion H, Mattisson T, Lyngfelt A. Solid fuels in chemical-looping combustion. Int J Greenh Gas Control 2008;2:180–93. doi:10.1016/S1750-5836(07)00117-X.

[23] Phyllis2, database for (treated) biomass, algae, feedstocks for biogas production and biochar n.d.

[24] Jenkins, B., Baxter, L., Miles, T. Jr., Miles T. Combustion properties of biomass, Fuel Processing Technology 54 1998:17–46.

[25] Keller M, Leion H, Mattisson T. Mechanisms of Solid Fuel Conversion by Chemical-Looping Combustion (CLC) using Manganese Ore: Catalytic Gasification by Potassium Compounds. Energy Technol 2013;1:273–82. doi:10.1002/ente.201200052.

[26] Mims CA, Pabst JK. Alkali-catalyzed carbon gasification kinetics: Unification of H2O, D2O, and CO2 reactivities. J Catal 1987;107:209–20. doi:10.1016/0021-9517(87)90286-7.

[27] Fennell P, Anthony B. Calcium and Chemical Looping Technology for Power Generation and Carbon Dioxide (CO2) Capture. Elsevier; 2015.

[28] Adánez J, De Diego LF, García-Labiano F, Gayán P, Abad A, Palacios JM. Selection of oxygen carriers for chemical-looping combustion. Energy and Fuels 2004;18:371–7. doi:10.1021/ef0301452.

[29] Johansson M, Mattisson T, Lyngfelt A. Comparison of oxygen carriers for chemical-looping combustion. Therm Sci 2006;10:93–107. doi:10.2298/tsci0603093j.

[30] Leion H, Mattisson T, Lyngfelt A. Energy Procedia Using chemical-looping with oxygen uncoupling (CLOU) for combustion of six different solid fuels. Energy Procedia 2009;1:447–53. doi:10.1016/j.egypro.2009.01.060.

[31] Arjmand M, Leion H, Mattisson T, Lyngfelt A. Investigation of different manganese ores as oxygen carriers in chemical- looping combustion (CLC) for solid fuels. Appl Energy 2014;113:1883–94. doi:10.1016/j.apenergy.2013.06.015.

[32] Sundqvist S, Khalilian N, Leion H, Mattisson T, Lyngfelt A. Manganese ores as oxygen carriers for chemical-looping combustion (CLC) and chemical-looping with oxygen uncoupling (CLOU). J Environ Chem Eng 2017;5:2552–63. doi:10.1016/j.jece.2017.05.007.

[33] Mattisson T, Linderholm C, Jerndal E, Lyngfelt A. Enhanced performance of manganese ore as oxygen carrier for chemical-looping with oxygen uncoupling (CLOU) by combination with Ca (OH) 2 through spray-drying. Biochem Pharmacol 2016;4:3707–17. doi:10.1016/j.jece.2016.08.006.

[34] Khan AA, de Jong W, Jansens PJ, Spliethoff H. Biomass combustion in fluidized bed boilers: Potential problems and remedies. Fuel Process Technol 2009;90:21–50. doi:10.1016/j.fuproc.2008.07.012.

[35] Wellinger M, Biollaz S, Wochele J, Ludwig C. Sampling and online analysis of alkalis in thermal process gases with a novel surface ionization detector. Energy and Fuels 2011;25:4163–71. doi:10.1021/ef200811q.

[36] Zevenhoven M, Yrjas P, Hupa M. Ash-Forming Matter and Ash-Related Problems. Handb. Combust., Weinheim, Germany: Wiley-VCH Verlag GmbH & Co. KGaA; 2010, p. 493–531. doi:10.1002/9783527628148.hoc068.

[37] Hupa M, Karlström O, Vainio E. Biomass combustion technology development - It is all about chemical details. Proc Combust Inst 2017;36:113–34. doi:10.1016/j.proci.2016.06.152.

[38] Knudsen JN, Jensen PA, Dam-Johansen K. Transformation and release to the gas phase of Cl, K, and S during combustion of annual biomass. Energy and Fuels 2004;18:1385–99. doi:10.1021/ef049944q.

[39] Davidsson KO, Korsgren JG, Pettersson JBC, Jäglid U. The effects of fuel washing techniques on alkali release from biomass. Fuel 2002;81:137–42. doi:10.1016/S0016-2361(01)00132-6.

[40] Johansen JM, Jakobsen JG, Frandsen FJ, Glarborg P. Release of K, Cl, and S during pyrolysis and combustion of high-chlorine biomass. Energy and Fuels 2011;25:4961–71. doi:10.1021/ef201098n.

[41] Tchoffor PA, Davidsson KO, Thunman H. Transformation and Release of Potassium, Chlorine, and Sulfur from Wheat Straw under Conditions Relevant to Dual Fluidized Bed Gasification 2013. doi:10.1021/ef401703a.

[42] Davidsson KO, Elled A-L, Eskilsson D, Leckner B, Åmand L-E, Steenari B-M. Countermeasures against alkali-related problems during combustion of biomass in a circulating fluidized bed boiler. Chem Eng Sci 2008;63:5314–29. doi:10.1016/j.ces.2008.07.012.

[43] Gu H, Shen L, Xiao J, Zhang S, Song T. Chemical looping combustion of biomass/coal with natural iron ore as oxygen carrier in a continuous reactor. Energy and Fuels 2011;25:446–55. doi:10.1021/ef101318b.

[44] Corcoran A, Marinkovic J, Lind F, Thunman H, Knutsson P, Seemann M. Ash properties of ilmenite used as bed material for combustion of biomass in a circulating fluidized bed boiler. Energy and Fuels 2014;28:7672–9. doi:10.1021/ef501810u.

[45] Pushp M, Gall D, Davidsson K, Seemann M, Pettersson JBC. Influence of Bed Material, Additives, and Operational Conditions on Alkali Metal and Tar Concentrations in Fluidized Bed Gasification of Biomass. Energy and Fuels 2018;32:6797–806. doi:10.1021/acs.energyfuels.8b00159.

[46] Markström P, Linderholm C, Lyngfelt A. Chemical-looping combustion of solid fuels - Design and operation of a 100kW unit with bituminous coal. Int J Greenh Gas Control 2013;15:150–62. doi:10.1016/j.ijggc.2013.01.048.

[47] Erbel C, Mayerhofer M, Monkhouse P, Gaderer M, Spliethoff H. Continuous in situ measurements of alkali species in the gasification of biomass. Proc Combust Inst 2013;34:2331–8. doi:10.1016/j.proci.2012.06.037.

[48] Sepman A, Ögren Y, Qu Z, Wiinikka H, Schmidt FM. Real-time in situ multi-parameter TDLAS sensing in the reactor core of an entrained-flow biomass gasifier. Proc Combust Inst 2017;36:4541–8. doi:10.1016/j.proci.2016.07.011.

[49] Zhang Z, Liu J, Shen F, Yang Y, Liu F. On-line measurement and kinetic studies of sodium release during biomass gasification and pyrolysis. Fuel 2016;178:202–8. doi:10.1016/j.fuel.2016.03.067.

[50] Porbatzki D, Stemmler M, Müller M. Release of inorganic trace elements during gasification of wood, straw, and miscanthus. Biomass and Bioenergy 2011;35:S79–86. doi:10.1016/j.biombioe.2011.04.001.

[51] Gall D, Pushp M, Davidsson KO, Pettersson JBC. Online Measurements of Alkali and Heavy Tar Components in Biomass Gasification. Energy and Fuels 2017;31:8152–61. doi:10.1021/acs.energyfuels.7b00474.

[52] van Lith SC, Jensen PA, Frandsen FJ, Glarborg P. Release to the gas phase of inorganic

elements during wood combustion. Part 2: Influence of fuel composition. Energy and Fuels 2008;22:1598–609. doi:10.1021/ef060613i.

[53] Corcoran A, Knutsson P, Lind F, Thunman H. Mechanism for Migration and Layer Growth of Biomass Ash on Ilmenite Used for Oxygen Carrier Aided Combustion. Energy & Fuels 2018;32:8845–56. doi:10.1021/acs.energyfuels.8b01888.

[54] Wiinikka H, Grönberg C, Öhrman O, Boström D. Influence of TiO2 additive on vaporization of potassium during straw combustion. Energy and Fuels 2009;23:5367–74. doi:10.1021/ef900544z.

[55] Henrik Leion, Pavleta Knutsson B-MS. Experimental Evaluation of Interactions between K, Ca, And P And Mn/Si-Based Oxygen Carriers. Eur. Biomass Conf. Exhib. Proc. Vol. 2017, Issue 25th EUBCE, June 2017, 2017, p. 660–5.

[56] Gyllén A. THESIS FOR THE DEGREE OF DOCTOR OF PHILOSOPHY Oxygen carrier aided combustion : Implementation of oxygen carriers to existing industrial settings. 2019.

[57] Novakovic´, AN, Van Lith SC, Frandsen FJ, Jensen PA, Holgersen LB. Release of Potassium from the Systems K-Ca-Si and K-Ca-P † n.d. doi:10.1021/ef8010417.

[58] Hildor F, Zevenhoven M, Brink A, Hupa L, Leion H. Understanding the Interaction of Potassium Salts with an Ilmenite Oxygen Carrier under Dry and Wet Conditions. ACS Omega 2020. doi:10.1021/acsomega.0c02538.